ChemMedChem

Chemistry Europe
European Chemical Societies Publishing

Accepted Article

Title: Design, synthesis, and computational study of hybrid quinazoline 1,3,5-triazines as epidermal growth factor receptor (EGFR) inhibitors with anticancer activity

Authors: Prateek Pathak, Hrvoje Rimac, Maria Grishina, Amita Verma, and Vladimir Potemkin

To be cited as: *ChemMedChem* 10.1002/cmdc.202000646

Link to VoR: https://doi.org/10.1002/cmdc.202000646

WILEY-VCH

WILEY-VCH

FULL PAPER

Design, synthesis, and computational study of hybrid quinazoline 1,3,5-triazines as epidermal growth factor receptor (EGFR) inhibitors with anticancer activity

Prateek Pathak,*[a] Hrvoje Rimac,*[a,b] Maria Grishina,[a] Amita Verma,[c] Vladimir Potemkin[a]

[a] Dr. P. Pathak, Dr. H. Rimac, Dr. M. Grishina, Dr. V. Potemkin
Laboratory of Computational Modelling of Drugs
South Ural State University
Chaikovskogo 20A, Chelyabinsk, 454008, Russia
patkhakp@susu.ru, rimatsk@susu.ru, grishinama@susu.ru, potemkinva@susu.ru

[b] Dr. H. Rimac
Department of Medicinal Chemistry
University of Zagreb Faculty of Pharmacy and Biochemistry
Ante Kovacica 1, Zagreb, 10000, Croatia
hrvoje.rimac@pharma.unizg.hr

[c] Dr. A. Verma
Bioorganic and Medicinal Chemistry Research Laboratory, Department of Pharmaceutical Sciences
Sam Higginbottom University of Agriculture, Technology & Sciences
Naini, Prayagraj, Uttar Pradesh 211007, India
amita.verma@shiats.edu.in

Abstract: We report a series of hybrid quinazoline-1,3,5-triazine derivatives as EGFR inhibitors, which were synthesized and tested using a variety of *in vitro, in silico,* and *in vivo* studies. The derivatives were found to be active against different cancer and non-toxic against normal cell lines, with compounds **7c**, **7d**, **7e**, and **7j** being the most potent ones. The derivatives were also evaluated for angiogenesis inhibition potency in chicken eggs and molecular docking and dynamics simulation studies were carried out to elucidate fundamental substituent groups essential for their bioactivity. Additionally, a SAR study of the derivatives was performed for future compound optimization. These studies suggested that the derivatives have a high affinity towards EGFR with favourable pharmacological properties. The most active compound (**7e**) was further evaluated for *in vivo* anticancer activity against DMBA induced tumour in female Sprague-Dawley rats as well as its effects on plasma antioxidant status, biotransformation enzymes, and lipid profile. The study suggested that the **7e** compound has lead properties against breast cancer and can serve as a starting compound for further development of anti-EGFR compounds.

Introduction

Several enzymes are involved in signal recognition, transduction and amplification and oversee cell growth and division. Among them, tyrosine kinases (TKs) are considered as one of the most significant ones[1,2] due to their versatile activity, such as cell proliferation, metabolism, and apoptosis. Therefore, irregularity in TK function is one of the mechanisms of tumour growth and progression.[3]

Based on their function, TKs can be categorized either as epidermal growth factor receptor (EGFR) or non-receptor kinases.[4] EGFR is a trans-membrane protein and belongs to the erbB/HER-family of TKs. These receptors consist of an extracellular ligand-binding domain, a cysteine-binding domain, an intracellular domain, and an alpha-helix transmembrane domain with TK activity within the carboxy-terminus (except for HER3).[5] EGFRs participate in transcription of regulatory molecules. Through their effects on cell proliferation, differentiation, apoptosis, invasion, and angiogenesis, a normal organ development takes place. EGFR signalling in tumour cells, as opposed to normal cells, is changed and often becomes dysregulated, where EGFR is overexpressed and/or obtains a gain-of-function mutation.[6–11] This behaviour leads to proliferation of tumour cells where they invade the surrounding tissue. This results in an increased angiogenesis.[12,13] Ras-Raf-mitogen activated protein kinase (MAPK) and phosphatidylinositol 3-kinase (PI3K)/Akt pathways[14] are the two main interconnected downstream pathways influenced by EGFR intracellular signalling. The over-expression of these signalling pathways acts as a driving force in advanced stages of malignant carcinogenesis (e.g. breast, colon, and bladder cancers, and some chordomas)[15–17] (Figure 1). Therefore, in rational drug design, EGFR inhibition is considered as one of the prime targets in cancer treatment.[18] As a result of intensive research, several EGFR inhibitors have been developed and are divided into generations based on their activity, e.g. erlotinib (Tarceva®)[17], vandetanib (Caprelsa®)[19], gefitinib (Iressa®)[20], lapatinib (Tykerb®, Tyverb®),[21] and the current state of the art, osimertinib (Tagrisso®)[22], to name a few (Figure 2A). EGFR inhibitors can either be reversible or irreversible, with reversible inhibitors binding in the ATP binding pocket and irreversible inhibitors binding either to the Cys 797 residue in the ATP binding pocket or to allosteric binding site(s).[23–26]

Quinazoline and 1,3,5-triazine scaffolds are important classes of *N*-heterocyclic compounds that have raised a great interest in cancer chemotherapeutics.[27–32] Our team has designed and synthesized a number of quinazoline based 1,3,5-triazine derivatives as effective TK inhibitors[31,32] (Figure 2B), where entire series of compounds exhibited significant activities (with IC_{50} ranging from 12.5 ± 0.01 to 43.30 ± 0.51 μM against MCF-7 and 8.8 ± 0.1 to 29.37 ± 0.08 μM against TPC-1 cell lines). It was found from the SAR studies that introduction of chloro-, bromo-, and nitro- groups into the phenyl ring improves the anticancer properties of the derivatives. Additionally, a 3D QSAR study concluded that the aliphatic bridge between the quinazoline and the 1,3,5-triazine ring acts as an antipharmacophoric group.

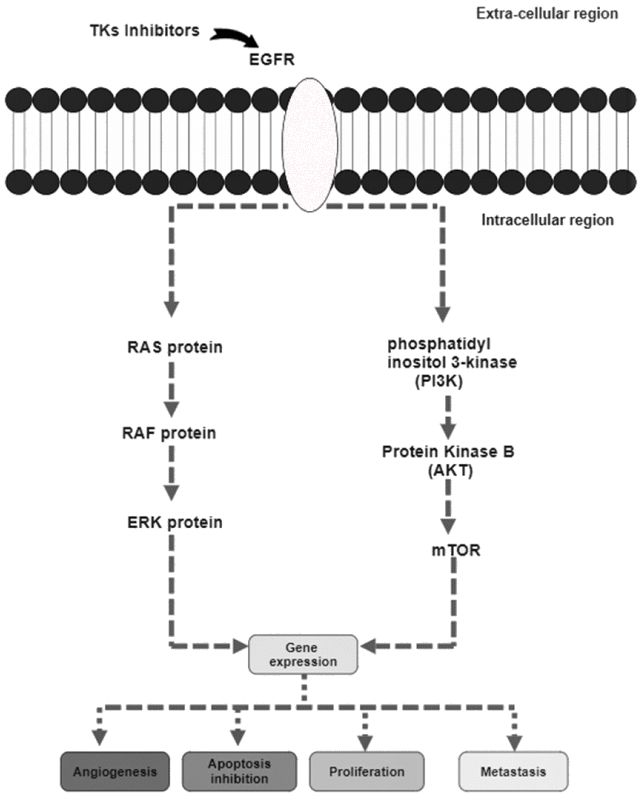

Figure 1. EGFR signalling pathway.

Further docking studies showed that the selectivity of molecules for TKs would be attained by making use of the supplementary hydrophobic pocket located in the back of the ATP-binding site by inclusion of other functional groups. The results were found to be similar to studies of other researches against kinase inhibitors.[33,34] Based on these results, in this research our attempt was to focus on the development of novel anticancer agents containing both the quinazoline and the 1,3,5-triazine rings.[31,32] This was obtained through molecular hybridization of the aforementioned rings, while the final molecules were obtained via substitution on the 1,3,5-triazine ring. The reasoning was that a substituted 1,3,5-triazine ring would fit nicely into the large hydrophobic cavity of the EGFR active site.

The evolution of EGFR inhibitors, as with all drugs in cancer treatment, is at least partly driven by cancer resistance to existing drugs. Therefore, having several structurally different compounds that bind to the same receptor could be beneficial in preventing cancer resistance or in cancer treatment after the resistance has already occurred.[35,36] Here we also mention in passing that there are two additional way of targeting EGFRs, by using monoclonal antibodies directed against the extracellular receptor domain, such as cetuximab,[37] or using PROteolysis TArgeting Chimeras (PROTACs). PROTACs are heterobifunctional molecules, which consist of a small molecule (binder to the protein target of interest), a ligand (recruiter of the E3 ligase), and a linker to conjugate the two moieties.[38,39] Binding of the PROTAC leads to selective polyubiquitination of the target protein and its subsequent degradation at the proteasome. This technology has been employed in degradation of numerous proteins[40–43], however, with a few exceptions,[23,44] targeting EGFR has not been extensively studied.[37]

Results and Discussion

Chemistry

We designed and synthesized a series of compounds by conjugating two different heterocyclic scaffolds, the 1,3,5-triazine and the quinazoline rings. The entire synthesis is shown in Scheme 1. The first step (reaction a) includes an acetylation reaction, where 2-amino-4,5-dibromo-benzoic acid (**1**) was refluxed with acetic anhydride and the intermediate compound 6,7-dibromo-2-methyl-benzo[d][1,3]oxazin-4-one (**2**) is obtained. In the next step (reaction b), compound **2** undergoes a nucleophilic substitution reaction in the presence of *p*-phenylenediamine. As a result, the oxygen atom from the oxazin-4-one ring in compound **2** is replaced by a nitrogen atom and compound **3** (3-(4-amino-phenyl)-6,7-dibromo-2-methyl-3H-quinazolin-4-one) is obtained. Another, parallel reaction (reaction c) is also carried out through a nucleophilic substitution of one of the chlorine atoms from cyanuric chloride (**4**) in the presence of piperidine, resulting in a formation of 2,4-dichloro-6-piperidin-1-yl-[1,3,5]triazine (compound **5**). Reaction d is also a nucleophilic substitution reaction where another chlorine atom of compound **5** is replaced by various aliphatic and aromatic amines. As a result, di-substituted 1,3,5-triazine derivatives (**6a-n**) were obtained. In the final step (reaction e), 3-(4-amino-phenyl)-6,7-dibromo-2-methyl-3H-quinazolin-4-one (**3**) and di-substituted 1,3,5-triazine derivatives (**6a-n**) are conjugated through a nucleophilic substitution reaction in the presence of tin as a catalyst and the derivatives (**7a-n**) are formed. Structural conformations of the derivatives were done by ^{1}H NMR, ^{13}C NMR and elemental analysis.

Anticancer activity

In vitro cytotoxicity of the entire series of the synthesized derivatives was evaluated for various cell lines, i.e. MCF-7 (breast cancer), HeLa (cervical cancer), HepG2 (hepatocellular carcinoma), HL-60 (human promyelocytic leukemia), HFF (human foreskin fibroblasts), and MCF-12A (normal epithelial cells) using the MTT assay, with erlotinib as reference. Erlotinib IC_{50} values are in accordance with its previously reported in-cell target engagement values,[15,45,46] which gives validity to the obtained results. IC_{50} values of all the derivatives were calculated and are displayed in Table 1. The **7a** derivative (with urea substituted 1,3,5-triazine ring) showed a marginal potency against MCF-7 (IC_{50} = 23.4 ± 0.1 μM), HeLa (IC_{50} = 24.2 ± 0.2 μM), HepG2 (IC_{50} = 35.4 ± 0.6 μM), and HL-60 (IC_{50} = 24.3 ± 0.1 μM), respectively. This potency was even more decreased by replacing urea with thiourea (**7b**). On the other hand, addition of an aromatic amine such as aniline (**7c**) improves the anticancer activity against all the selected cancer cell lines. Additionally, the anticancer potency was marginally increased (except for HepG2) by introduction of chlorine in the phenyl ring (**7d**). This indicates that incorporation of a group that resonantly donates electrons (e.g. Cl) in the phenyl ring improves potency against breast and leukemic cancers. Replacement of the *p*-chloro-aniline group by a morpholine ring (**7e**) additionally improves the activity against all tested cell lines (MCF-7 (IC_{50} = 17.2 ± 0.1 μM), HeLa (IC_{50} = 17.3 ± 0.1 μM), HepG2 (IC_{50} = 15.1 ± 0.2 μM), and HL-60 (IC_{50} = 14.3 ± 0.1 μM)),

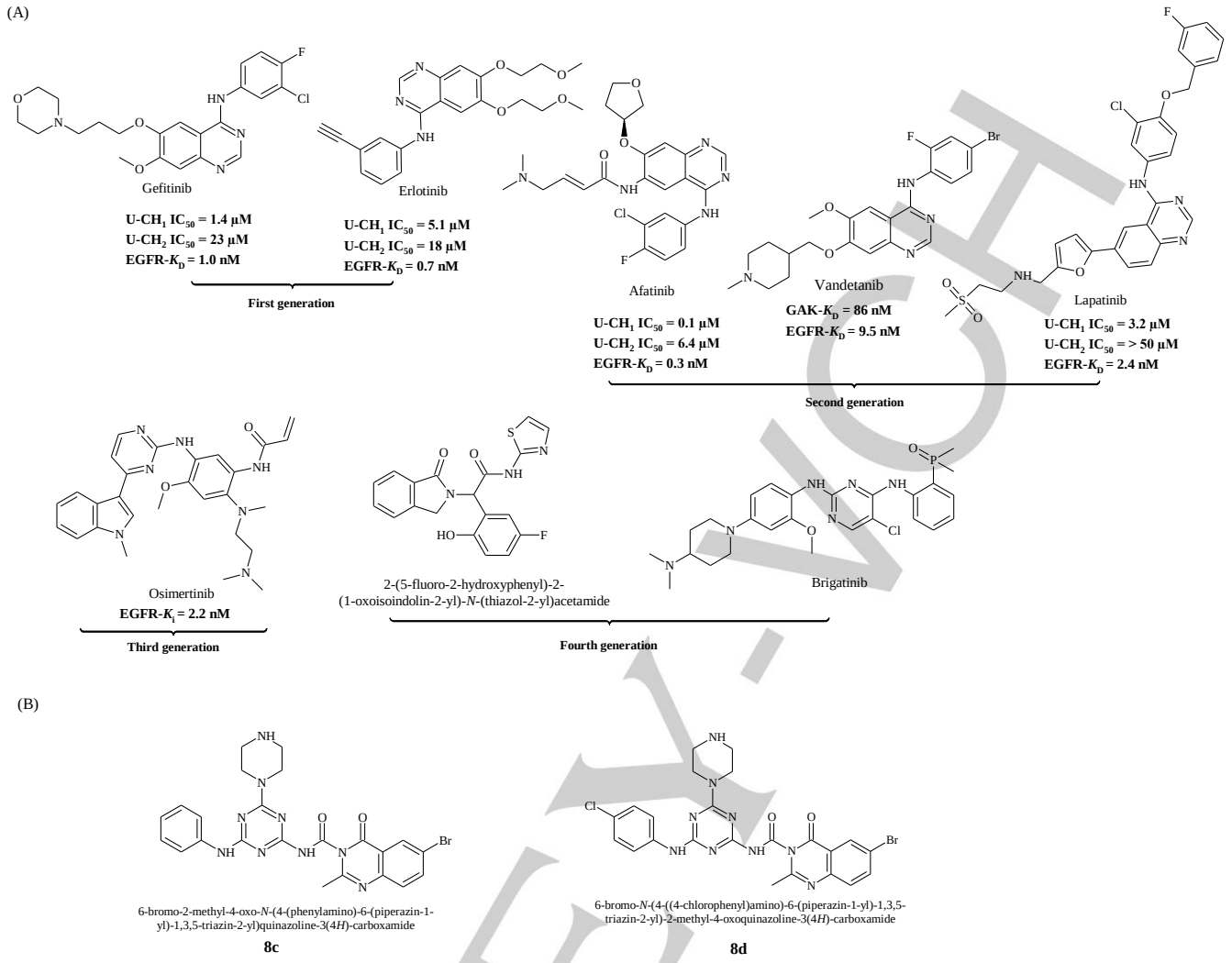

Figure 2. (A) Tyrosine kinase (EGFR) inhibitors[15,47,48], and (B) the most active compounds previously synthesized by our team.

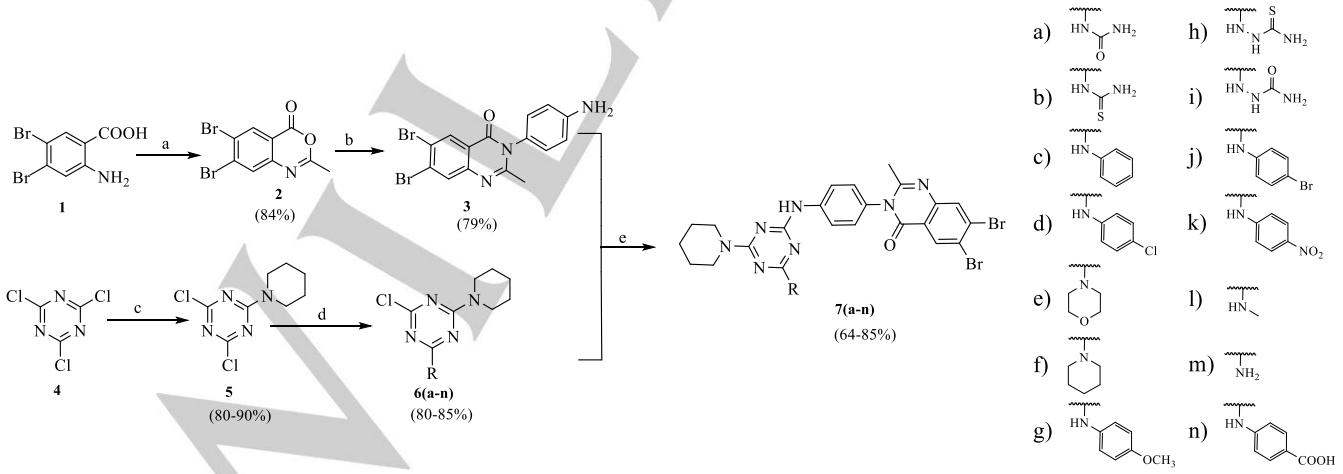

Scheme 1. The reaction scheme for the synthesized derivatives: a) acetic anhydride, reflux for 4 hours, b) *p*-phenylenediamine, pyridine, reflux for 3 hours, c) piperidine, acetone, $NaHCO_3$ (10%), stir for 3-4 hours below 5 °C, d) various amines, acetone, $NaHCO_3$ (10%), stir for 4 hours at room temperature, e) 1,4-dioxane, K_2CO_3, tin granules, reflux for 6-8 hours.

but a piperidine ring (**7f**) lowers potency against all tested cell lines. This further confirms that the presence of electron donating substituents (in this case oxygen, and, in the case of derivative **7d**, chlorine) increases the anticancer potency. A derivative with a methoxy-aniline substituted 1,3,5-triazine ring (**7g**) showed a slight decrease in anticancer potency, compared to compounds **7e** and other aniline substituted derivatives (**7c** and **7d**), but was found to be more potent than compounds with an aliphatic substitution, such as **7a** and **7b**. Further, compounds **7h** and **7i** (thiosemicarbazide and semicarbazide substituted 1,3,5-triazine derivatives, respectively) had a significantly lower activity against all tested cell lines, probably due to their basic nature or simply due to their polarity. In compounds **7j** and **7k** (bromo- and nitro-substituted 1,3,5-triazine derivatives, respectively) we can again see the role of an aromatic substitution, which increases anticancer potency (not applicable for the **7n** derivative and its *p*-amino benzoic acid (PABA) substituent). Briefly, thiourea, methylamino, amino, and PABA substituted derivatives **7b**, **7l**, **7m**, and **7n** expressed the lowest efficacy among the entire series, while derivatives **7c**, **7d**, **7e**, and **7j** were found to be the most active. The assays also showed that the potency of some derivatives (especially derivative **7e**) is very similar to erlotinib's potency, even though erlotinib still remained the most active compound. A closer look into the structure-activity relationship shows that introduction of open aliphatic amino functional groups, such as in derivatives **7a**, **7b**, **7h**, **7i**, **7l**, and **7m** results in a slightly lower anticancer efficiency as compared to aromatic substitutions on the 1,3,5-triazine ring (**7c**, **7d**, **7j**, and **7k**), which is in accordance with a previous study.[15] Additionally, it was illustrated that the presence of an electronegative group (i.e. Cl, Br, and NO_2) is crucial for the activity. This was also shown by Srivastava *et al.*, who determined that presence of electron withdrawing groups with a halogen (fluoro-anilino group) on the triazine scaffold is necessary for the anticancer activity. Furthermore, they concluded that the presence of an electron donating group composed of non-halogen substituents significantly decreases the anticancer efficacy.[49] This is in accordance with our study, which has demonstrated that a halogen containing phenyl ring (bromo- and nitro-phenyl groups) acts as a key fragment in increasing the anticancer potential. These results show an interesting connection between substituents and their anticancer activity. The selectivity of the derivatives between normal and cancerous cells was also evaluated using two normal cells lines (HFF and MCF-12A) and the results showed that most of the derivatives (not including **7g**, **7j**, and **7n** at higher concentrations) were non-toxic for normal cell lines (Table 1).

EGFR inhibitory activity

In vitro EGFR inhibition was performed for the entire set of derivatives and results are given as IC_{50} and compared to the reference drug (erlotinib) (Table 2). It can be seen that some derivatives have a moderate to excellent inhibitory potential, with derivatives **7e**, **7j**, and **7d** being the most potent (with IC_{50} = 36.8 ± 0.5 nM, 36.6 ± 0.8 nM, and 41.0 ± 0.7 nM, respectively). Furthermore, a slightly lower inhibition was reported for the **7c** (IC_{50} = 49.6 ± 0.4 nM) and **7k** (IC_{50} = 58.8 ± 0.6 nM) derivatives. For derivatives **7f** and **7g**, IC_{50} decreases to 65.2 ± 0.8 nM and 68.9 ± 0.5 nM respectively, followed by derivatives **7a**, **7b**, **7h**, **7i**, **7l**, **7m**, and **7n** (IC_{50} > 100 nM in all cases). Erlotinib's IC_{50} was found to be 31 nM, which is in accordance with earlier studies,[32] and allows comparison of our results with results of other studies.[15] This study also suggests that introduction of an electronegative group helps to improve the anti-EGFR activity, very similarly to the *in vitro* anticancer activity assay. Even though

Table 1. *In vitro* anticancer effect of the synthesized derivatives in selected cell lines.

Derivative	*In vitro* anticancer activity (IC_{50} in μM)					
	MCF-7	HeLa	HepG2	HL60	HFF	MCF-12A
7a	23.4 ± 0.1	24.2 ± 0.2	35.4 ± 0.6	24.3 ± 0.1	> 100	> 100
7b	36.0 ± 0.4	24.7 ± 0.1	43.3 ± 0.2	26.3 ± 0.2	> 100	> 100
7c	18.7 ± 0.2	19.2 ± 0.2	15.8 ± 0.3	16.9 ± 0.2	> 100	> 100
7d	18.2 ± 0.5	18.0 ± 0.5	16.5 ± 0.1	16.5 ± 0.3	> 100	> 100
7e	17.2 ± 0.1	17.3 ± 0.1	15.1 ± 0.2	14.3 ± 0.1	> 100	> 100
7f	19.6 ± 0.2	20.5 ± 0.4	18.5 ± 0.1	18.2 ± 0.1	> 100	> 100
7g	21.5 ± 0.2	22.0 ± 0.6	19.0 ± 0.1	21.2 ± 0.1	74.0 ± 0.1	78.9 ± 0.7
7h	23.7 ± 0.4	23.2 ± 0.2	36.8 ± 0.4	24.8 ± 0.4	> 100	> 100
7i	22.5 ± 0.2	24.4 ± 0.1	30.8 ± 0.2	22.2 ± 0.2	> 100	> 100
7j	17.8 ± 0.4	17.5 ± 0.1	15.2 ± 0.1	14.8 ± 0.1	78.6 ± 0.4	> 100
7k	19.4 ± 0.1	20.3 ± 0.1	12.7 ± 0.3	18.6 ± 0.1	> 100	> 100
7l	39.5 ± 0.5	32.2 ± 0.1	45.4 ± 0.4	30.2 ± 0.1	> 100	> 100
7m	25.7 ± 0.2	24.3 ± 0.3	32.5 ± 0.6	22.8 ± 0.4	> 100	> 100
7n	25.3 ± 0.2	25.4 ± 0.4	36.7 ± 0.4	25.0 ± 0.1	72.6 ± 0.5	78.1 ± 0.5
Erlotinib	16.7 ± 0.7	17.3 ± 0.2	12.6 ± 0.1	13.7 ± 0.3	70.1 ± 0.5	> 100

the inhibition of other kinases (off-target effects) was not tested and therefore cannot be excluded, based on the similarity of anti-cancer activity and EGFR inhibition results, it can be safe to say that the synthesized derivatives engage the EGFR and produce their anticancer activity mostly through its inhibition. While the EGFR IC_{50} values reflect the intrinsic sensitivity of the enzyme to the inhibitors, the IC_{50} values obtained for different cell lines are a result of a complicated interplay between the inhibitors and the cells, involving different physical, chemical and biological factors, resulting in lower inhibitor activity.[15,50–52] Additional effects of the **7e** compound are discussed in the "*In vivo* pharmacology" section.

Antiangiogenic activity in MCF-7 inoculated chicken CAM

Since migration of cancer cells enhances the number of newly formed blood vessel branch points compared to the PBS-treated control group, the synthesized 1,3,5-triazine derivatives (at concentration of 0.01 nM) were evaluated for their antiangiogenic activity against MCF-7 inoculated chicken embryos. The results are reported in term of score (Figure 3), as described in the Experimental Section. The entire set of derivatives showed moderate to significant angiogenesis inhibition scores (from 0.6 ± 0.1 to 1.9 ± 0.1), compared to erlotinib, which had a score of 1.87 ± 0.03. Briefly, the **7e** derivative, which was found to be the most promising compound in the MTT and EGFR assays, was also the most potent in this assay, with a score of 1.90 ± 0.06. This was followed by derivatives **7j** (1.90 ± 0.02), **7d** (1.84 ± 0.02), **7c** (1.82 ± 0.07), and **7k** (1.50 ± 0.07). The rest of the derivatives showed either moderate or low inhibition (~50%) compared to erlotinib, with derivative **7l** being the least potent one (0.6 ± 0.1). As in the previous results, these results also demonstrate the importance of cyclic amine substituents (such as morpholine and piperidine rings) or electron donating groups in the 1,3,5-triazine scaffold, as opposed to the open chain aliphatic amino groups.

Table 2. IC_{50} values and docking results for EGFR inhibition by synthesized derivatives.

Derivative	IC_{50} (nM)	K_{BIND} (kcal/mol)
7a	197.2 ± 0.8	-10.0
7b	255.1 ± 0.8	-9.6
7c	49.6 ± 0.4	-11.4
7d	41.0 ± 0.7	-11.6
7e	36.8 ± 0.5	-11.4
7f	65.2 ± 0.8	-11.1
7g	68.9 ± 0.5	-11.1
7h	201.1 ± 0.6	-9.9
7i	108.1 ± 0.4	-10.4
7j	36.6 ± 0.8	-11.7
7k	58.8 ± 0.6	-11.2
7l	108.2 ± 0.4	-9.4
7m	178.4 ± 0.9	-10.1
7n	246.2 ± 0.6	-9.9
erlotinib	31.1 ± 0.5	-10.9

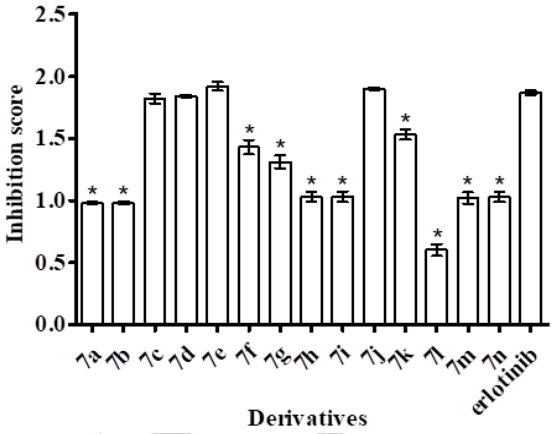

Figure 3. Antiangiogenic activity of synthesized derivatives at 0.01 nM against MCF-7 inoculated CAM. Derivatives marked with asterisk (*) have a statistically different ($p < 0.05$) inhibition score than erlotinib.

Docking studies

First, redocking of erlotinib was performed using the 4HJO PDB structure (resolution 2.75 Å). However, a relatively weak binding constant (-7.9 kcal/mol) with a non-correct pose was found, and erlotinib in the correct crystallographic pose was found to bind with a binding constant of -6.6 kcal/mol. Docking of erlotinib was also tried with the 1XKK structure, but yielded another incorrect pose, but with identical binding constant of -7.9 kcal/mol. This shows that the docking procedure was not able to correctly determine the correct pose and binding energy of erlotinib, probably due to its flexible aliphatic chains. Since the tested derivatives are more similar to lapatinib, redocking of lapatinib was also tried for the 1XKK complex. Comparison of the redocked pose with the crystallographic structure is shown in Figure 4. As can be seen, there is virtually no difference between lapatinib redocked poses obtained under different docking settings (tan) and their energies (ranging from -11.0 to -10.7 kcal/mol) and the crystallographic pose (light blue). The most significant difference is in the orientation of the flexible chain which is located outside

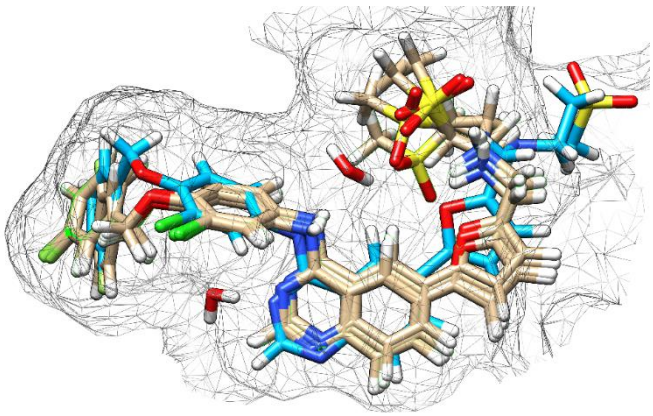

Figure 4. Docked poses of lapatinib in its charged and neutral state and without water molecules and in presence of HOH 4 and HOH 22 water molecules (tan) compared to the lapatinib's crystallographic orientation (light blue).

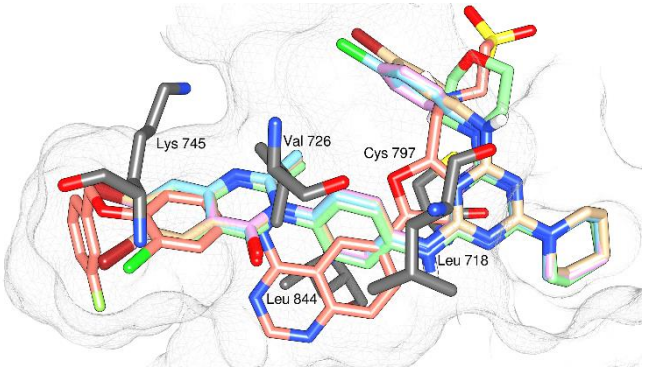

Figure 5. Comparison of the best docking poses for ligands **7j** (tan), **7d** (light blue), **7c** (pink), and **7e** (green) with crystallographic structure of lapatinib (red) and five of the most important amino acid residues (gray).

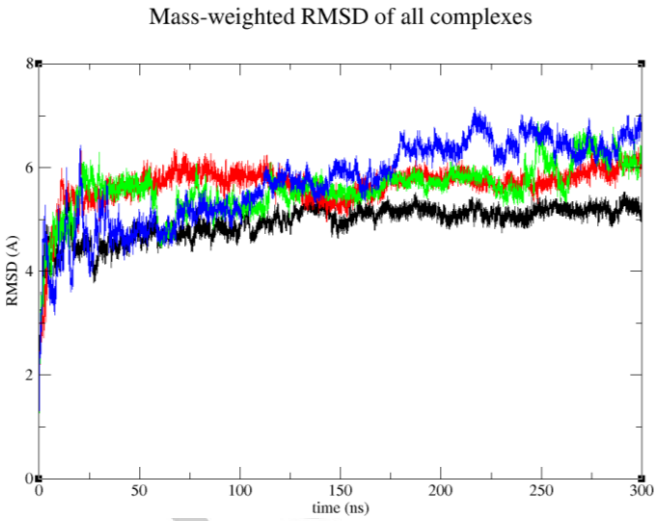

Figure 6. Mass weighted root-mean-square deviation (RMSD) through time for ligands **7j** (black), **7d** (red), **7c** (green), and **7e** (blue) bound to EGFR.

of the binding pocket. Due to this, docking of other ligands was conducted in their most prevalent moieties at pH 7.4, but in absence of all water molecules. Under these conditions, the calculated lapatinib binding energy was -10.9 kcal/mol. Docking results for other ligands are shown in Figure 5 and Table 2. It is immediately noticeable that there is no significant difference in their poses. This is expected, as the difference in their structures is also minimal. The most significant difference can be seen in the case of ligand **7e** and its morpholine ring. Compared to the other three ligands, which have an (un)-substituted phenyl ring, morpholine ring is neither planar nor aromatic and is also bulkier. However, this does not pose a major disadvantage in binding because, as can be seen from Figure 5, the part of the binding site which accommodates these substituent groups is not buried inside the protein. These obtained docking poses (erlotinib and ligands **7c**, **7d**, **7e**, and **7j**) were then used in MD simulations to check the validity of the obtained results, as docking can sometimes deliver unstable poses,[32] as well as to determine the contribution of individual amino acid residues to ligand binding.

MD simulations

Both docked erlotinib poses (using 1XKK and 4HJO EGFR conformations) underwent MD simulations to see if they will converge and be comparable with the crystallographic structure. This was found to be true (data not shown), further emphasizing the fact that one should be careful while interpreting docking results. Additionally, these results validate the approach of using MD simulations in obtaining correct binding poses for both erlotinib and synthesized ligands, as well as in obtaining further insight into their interactions with EGFR. Figure 6 shows mass-weighted root-mean-square deviation (RMSD) of all four complexes through time. It can be seen that some complexes achieve equilibrium state earlier (**7j** and **7d**), while for other complexes it takes more time (**7c** and **7e**). The graph also indicates that in the case of the complex with the **7e** ligand, the most significant protein conformation change occurs, compared to other ligands (discussed later). The lowest RMSD values are found for the complex with the **7j** ligand. This can also be seen in the intermolecular H-bond graph (Figure 7). For the **7j** ligand the number of intermolecular H-bonds is relatively stable for the entire duration of the simulation (with a fast drop in number of H-bonds at the beginning of the simulation). The behaviour of complexes with ligands **7d** and **7c** is similar, the only difference is that it takes them more time to achieve the equilibrium state. However, in the case of the complex with ligand **7e**, the number of H-bonds increases over time (also discussed later). Binding energies for all complexes were calculated using the MM-GBSA protocol (Table 3) to obtain a further insight into the EGFR-ligand binding. While in the docking studies, binding affinity decreased in the order **7j** > **7d** > **7c** > **7e**, in the MD simulations the order is **7e** > **7j** > **7d** > **7c** (while erlotinib's affinity was calculated to be -49.82 kcal/mol, and is situated between compounds **7e** and **7j**, for complete MM-GBSA results see Supplementary Information).

From Table 3 it can be seen that all 4 derivatives have very similar interactions with nearby amino acid residues, but what differentiates the **7e** derivative are its stronger hydrophobic interactions with the two most contributing residues, Leu 718 and Val 726, as well as a much stronger interaction (mostly van der Waals and electrostatic in nature) with the Cys 797 residue (0.8 – 1.18 kcal/mol stronger interaction compared to the other three residues). This residue was previously identified as the key residue and is the target of covalent EGFR inhibitors.[24,53–55] Interactions with other key residues, such as Lys 745, Thr 790, and Thr 854 seem to be approximately of the same strength. These residues were recognized as key residues in lapatinib binding,[56] as well as binding of other EGFR inhibitors.[15,45,46,57] As a side note, it has to be pointed out that the calculated ΔG_{bind} is overestimated in absolute terms, which is a known limitation of the MM-GBSA method.[58] This fact was extensively discussed by Homeyer and Gohlke,[59] which pointed out that, despite this drawback, the method has a huge potential in predicting relative binding energies in biomolecular complexes and can be used to compare relative binding energies of structurally similar compounds, as it is in this case. For this reason, the obtained ΔG_{bind} of tested compounds should only be analysed relative to each other.[24,53–55]

The discrepancy in the binding affinities obtained through docking and MD simulations can be explained by the RMSD and H-bond data. The protein conformation obtained by X-ray crystallography favours binding of ligand **7e** the least (compared to the other three ligands), but if we let EGFR obtain its natural conformation in a water solution through MD simulations, its conformation will change in a way that favours **7e** binding the most. This

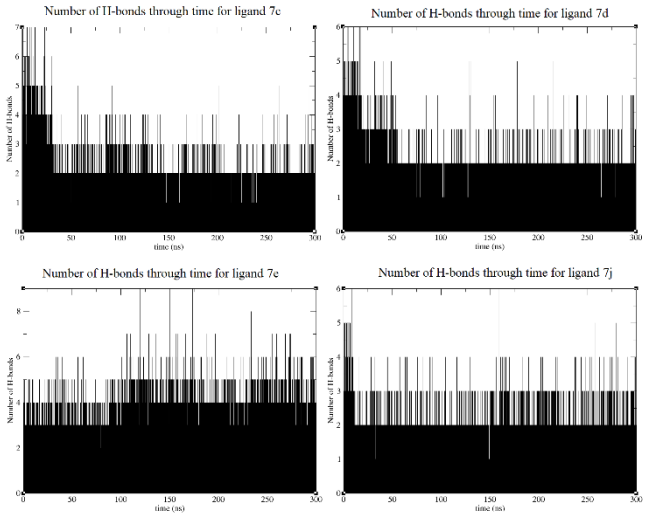

Figure 7. Number of intermolecular hydrogen bonds through time for the best four complexes.

conformational change is reflected in higher RMSD values for the **7e** complex. Additionally, at the beginning of the simulation, the number of intermolecular H-bonds for the **7e** complex is the lowest (the least favourable binding), but we can see that the number of intermolecular H-bonds increases over time (while for the other 3 complexes it decreases from the initial value). If we consider the entire time of the simulations, the average number of H-bonds for the **7e** ligand is more than 3 times higher than for the rest of the complexes, regardless of the initial lowest value (the average number of intermolecular H-bonds decreases in order **7e** (1.07 ± 0.95) > **7c** (0.29 ± 0.64) > **7d** (0.28 ± 0.59) > **7j** (0.23 ± 0.54)). This confirms the importance of enzyme conformation: crystallographic conformation of the enzyme was suboptimal for binding of the **7e** ligand, resulting in the lowest affinity among the tested ligands. However, in the MD simulations, since the enzyme is not constrained, it will adapt a conformation that lowers the energy of the whole complex by, among other things, forming additional H-bonds which are not present in the initial crystallographic enzyme conformation, as can be seen in Figure 8. This fact also emphasizes the importance of choosing the most appropriate protein conformation for docking studies, i.e. among other points to consider (such as resolution of the PDB structure, missing side chains, clashes, Ramachandran outliers, etc.), one should ensure that the ligand from the PDB structure is structurally as similar as can be with the tested ligands to ensure the appropriateness of the binding site conformation and the validity of the results.

If we compare ligand poses after docking (Figure 5) and after MD simulations (Figure 8), we can see that the quinazoline part of the ligands, which is inside the binding pocket, has virtually the same conformation in all the ligands. As for the parts which are located outside of the binding site, for ligands **7j**, **7d** and **7c**, they remain in the same orientation as in the docking studies, but in the case of ligands **7e**, this part of the molecule is rotated by approximately 180°. This is enabled by the change in the secondary structure of protein residues 991–1012 (Figure 8A) and 718–723 (Figure 8B). In the case of the complex with ligand **7j**, residues 991–1012 are located the closest to the binding pocket, compared to the other complexes. Complexes with ligands **7c** and **7d** are intermediate cases, and in the case of the **7e** ligand these residues are located the farthest away, enabling the rotation of the molecule and much more favourable interactions. This rotation is additionally supported by a change in conformation of residues 718–723 (Figure 8B). In the case of complex with the **7e** ligand, these residues are located closer to the ligand, resulting in bad contacts and favouring the rotation of this part of the ligand. This can be seen especially in the case of Gly 719: while its contribution to ligand binding is significant for ligands **7j**, **7d** and **7c** (-0.85 – -1.21 kcal/mol), for ligand **7e** binding it has a less significant role (-0.16 kcal/mol). Additionally, all other residues in this segment (residues 718–723) slightly disfavour ligand **7e** binding.

Table 3. Contribution of top ten individual residues to ΔG_{bind} (kcal/mol) of tested ligands to EGFR.

Derivative **7c**		Derivative **7d**		Derivative **7e**		Derivative **7j**	
Total	**-41.8**	Total	**-43.27**	Total	**-52.79**	Total	**-46.65**
Leu 718	-2.9	Leu 718	-2.83	Leu 718	-2.95	Leu 718	-2.60
Val 726	-2.2	Lys 745	-2.22	Val 726	-2.62	Val 726	-2.51
Lys 745	-2.0	Val 726	-2.13	Cys 797	-2.50	Lys 745	-2.16
Cys 797	-1.7	Cys 797	-1.59	Leu 844	-1.67	Leu 844	-1.55
Leu 844	-1.6	Leu 844	-1.54	Lys 745	-1.66	Thr 854	-1.32
Thr 854	-1.3	Thr 854	-1.34	Gly 796	-1.65	Cys 797	-1.31
Leu 788	-1.1	Thr 790	-1.11	Thr 790	-1.26	Gly 719	-1.21
Gly 719	-1.0	Leu 788	-1.03	Thr 854	-1.19	Thr 790	-1.08
Ala 743	-0.9	Ala 743	-0.91	Ile 744	-1.18	Leu 788	-1.08
Thr 790	-0.9	Gly 719	-0.85	Ala 743	-1.04	Ser 720	-1.06

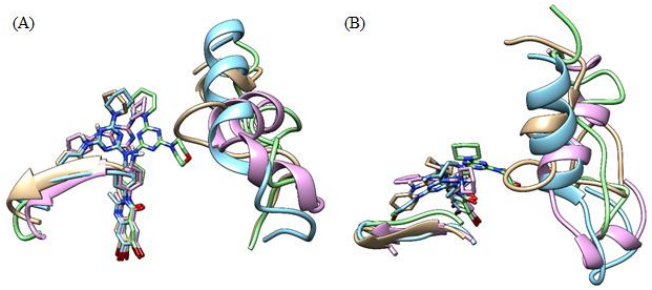

Figure 8. Poses of EGFR-ligand complexes after MD simulations with secondary structure of protein residues 718–723 and 991–1012 shown. **7j** complex is depicted in tan, **7d** in light blue, **7c** in pink, and **7e** in green: A) side view, B) top view.

In summary, stronger binding of the **7e** ligand compared to the other three derivatives is mostly a result of a much stronger interactions with the key Cys 797 residue, as well as conformational EGFR changes brought about by the introduction of the morpholine ring, which is not present in the case of the other ligands.

Using SAR, docking and MD results, a valuable insight into the pharmacophoric and physicochemical characteristics was obtained. This will form a basis for further development of novel hybrid quinazoline 1,3,5-triazines with even higher potency.

In vivo pharmacology

Effect on body weight, percentage of tumour incidence and tumour volume

In vitro anticancer activity, EGFR inhibitory activity, *in ovo* angiogenesis inhibition, and docking and molecular dynamics results of the **7e** derivative encouraged us to further examine its *in vivo* activity. Therefore, we utilized 7,12-dimethylbenz(a)anthracene (DMBA) to induce mammary cancer in experimental animals to validate the defensive effect of the **7e** derivative. These effects were shown as an influence on body weight of experimental animals (Figure 9A). The DMBA induced group displayed a substantial decline in body weight as compared to the control group. In the treated groups, body weight of the animals has notably improved in a dose-dependent manner. Additionally, the **7e** derivative was also evaluated based on the tumour volume and tumour incidence percentage (Figure 9B and 9C), which showed that the **7e** derivative has exceptional efficiency in reducing both tumour incidence and its volume. This suggests that it has a broad and significant activity against mammary cancer.

Effect on enzymatic and non-enzymatic antioxidants

This study aimed to determine the effect of the **7e** derivative on the antioxidant status in plasma and mammary tissue of experimental animals. Various studies established that antioxidants act as a crucial defence system against cancer.[60] Therefore, anti-breast cancer efficiency of the **7e** derivative can be also examined through the study of the endogenous antioxidant system because in various stages of cancer, the antioxidant system is greatly deregulated and compromised. The results showed significant changes ($p < 0.001$) in chloramphenicol acetyltransferase (CAT), glutathione peroxidase (GPX), glutathione (GSH), and superoxide dismutase (SOD) levels

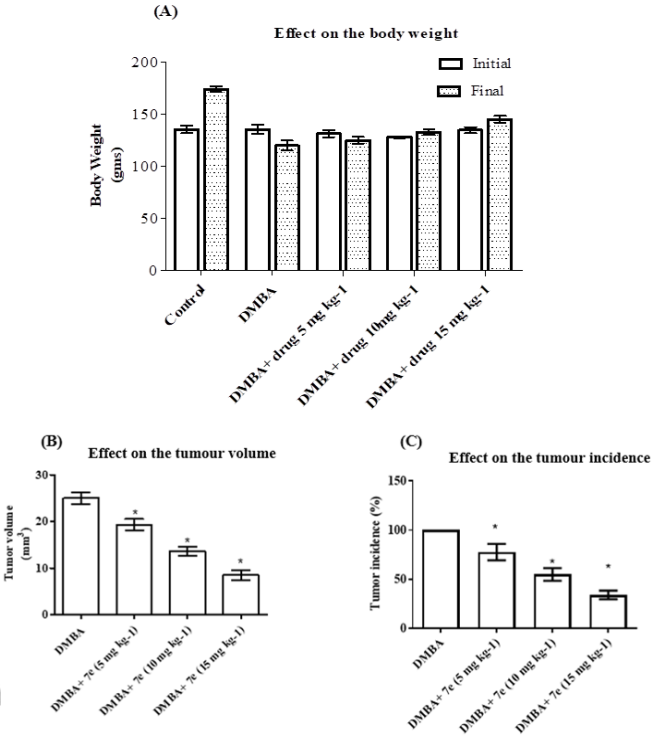

Figure 9. Effect of the **7e** derivative on the body weight (A), tumour incidence (B), and tumour volume (C) in different animal groups. A statistically significant difference in tumour volume and incidence ($p < 0.001$) from the control is marked by an asterisk (*).

(Figure 10(A-D) and 11(A-D), respectively). These results clearly show that the level of these enzymes in DMBA induced group was significantly reduced ($p < 0.001$), compared to the control. Additionally, the treated groups showed significant improvement ($p < 0.001$) in the antioxidant status. Further, the correlation study with tumour incidence and volume suggested that the **7e** derivative displays extensive protective properties against breast cancer probably via scavenging of free radicals. Lipid peroxidation parameters such as lipid hydroperoxides (LOOH) and thiobarbituric acid reactive substances (TBARS) extensively influence production of reactive oxygen species (ROS), play a considerable role in the tumour progression, and are considered critical in peroxidation of membrane lipids. For that reason, levels of LOOH and TBARS were also measured (Figures 10(E-F) and 11(E-F), respectively). It can be clearly seen that in the DMBA treated animal groups, LOOH and TBARS levels are significantly elevated ($p < 0.001$), compared to the control group. So, the **7e** derivative actively participates in lowering the levels of these markers and is correlated with an increase of antioxidant parameters. In a study by Karki *et al.*, it was established that the free radical generation is a major cause of cell damage, with enzymatic and non-enzymatic antioxidants acting as protective mechanisms.[60] In the present study, we also observed this phenomenon. As the **7e** derivative decreases the levels of free radicals and oxidative stress, it has an additional benefit, and can also serve as an indicator of cancer chemotherapy efficiency.

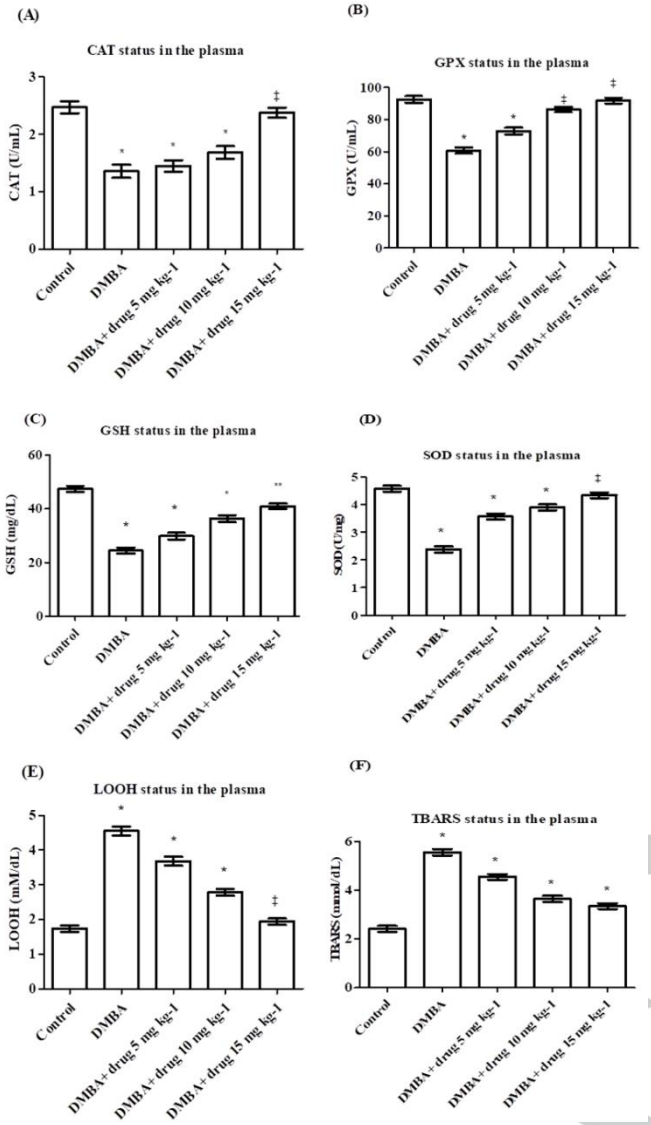

Figure 10. Effect of the **7e** derivative on the plasma antioxidant status of treated animals. A statistically significant difference in means in comparison to control is marked by a symbol: * $p < 0.001$, ** $p < 0.01$, ‡ $p > 0.05$.

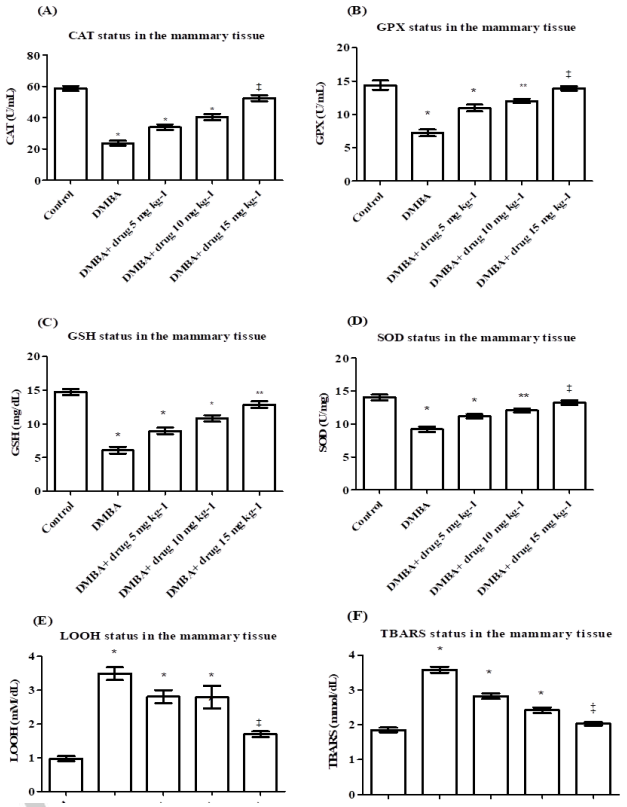

Figure 11. Effect of the **7e** derivative on the antioxidant status in the mammary tissue of treated animals and control. A statistically significant difference in means in comparison to control is marked by a symbol: * $p < 0.001$, ** $p < 0.01$, ‡ $p > 0.05$.

Effects on biotransformation enzymes in liver microsomes and in mammary tissue

Metabolic enzymes are involved in the biotransformation process and excretion of by-products generated by cancer causing agents. It was observed that DMBA metabolism is influenced by CYP and other phase I enzymes. These metabolites have a major role in the induction of cancer and its related effects. Additionally, biotransformation enzymes, such as GST and GR, which are involved in the phase II metabolism, convert DMBA into water soluble conjugates.[49] Due to this, excretion of these metabolites increases, and this acts as a protective mechanism in cancer prevention. So, it was crucial to also see if the **7e** derivative has any influence on these enzymes. Expression of liver and mammary tissues biotransformation enzymes, such as phase I (cytochrome P450 (CYP), cytochrome-b5 (Cyt-b5)) and phase II (glutathione S-transferase (GST), glutathione reductase (GR)) enzymes, in the treated and control animals are displayed in Figures 12 and 13. The level of CYP and Cyt-b5 enzymes were significantly higher ($p < 0.001$) in the DMBA treated group, compared to the control group. However, level of GST and GR enzymes were found to be significantly reduced ($p < 0.001$). The drug treated group of animals illustrated a dose dependent decline in the level of phase I enzymes (CYP and Cyt-b5) in liver and in mammary tissue. Moreover, a significant rise ($p < 0.001$) in GST and GR levels was reported in liver and mammary tissue. These results imply that the **7e** derivative has a notable role in the modulation of levels of phase I and phase II enzymes.

Effect on the lipid profile level

This segment of the study included a comparison of lipid profiles such as triglycerides (TG), total cholesterol (TC), high-density lipoproteins (HDL), low-density lipoproteins (LDL), and very-low-density lipoprotein (VLDL) (Figure 14). Since higher level of triglycerides and LDL are associated with cancer and metastasis,[61] levels of these parameters were measured and found to be significantly elevated ($p < 0.001$) in the DMBA treated group, whereas they were decreased in the **7e** treated group in a dose dependent manner.

Conclusion

We report a synthesis of a series of hybrid quinazoline-1,3,5-triazine derivatives and their anticancer activity. Pharmacological evaluation indicated that substitution of the 1,3,5-triazine ring by morpholine and aniline rings and their derivatives increases

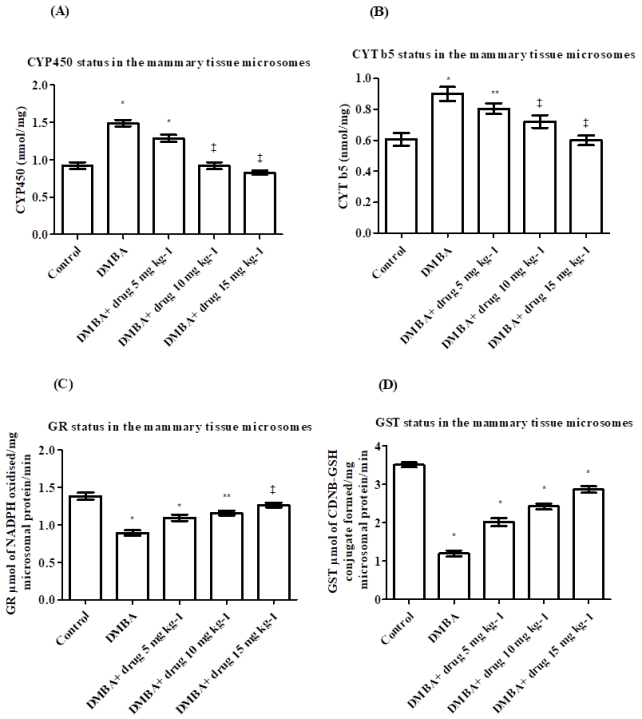

Figure 12. Effect of the **7e** derivative on the level of biotransformation enzymes in mammary tissue microsomes of treated and control group. A statistically significant difference in means in comparison to control is marked by a symbol: * $p < 0.001$, ** $p < 0.01$, ‡ $p > 0.05$.

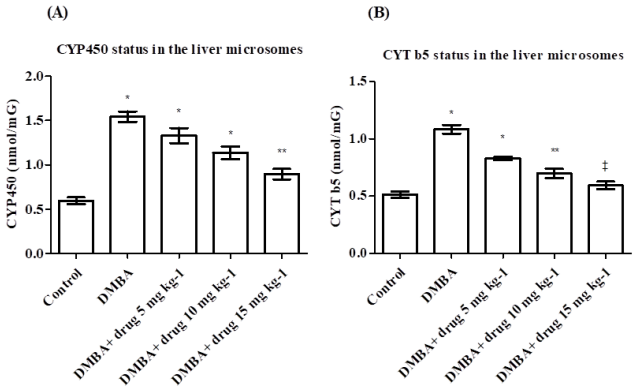

Figure 13. Effect of the **7e** derivative on the level of biotransformation enzymes in liver microsomes of treated and control animal groups A statistically significant difference in means in comparison to control is marked by a symbol: ** $p < 0.001$, * $p < 0.01$, # $p < 0.05$, and ‡ $p > 0.05$.

ligand potency in EGFR inhibition. Further, 3D QSAR studies confirmed that introduction of aniline and its respective variants is a potential way to increase the biological activity through improving pharmacophoric properties. MD studies have shown that all the tested ligands bind very strongly in the EGFR active pocket, which is in accordance with the experimental results. Their orientation in the active site is also quite similar, with only exception being the **7e** ligand. MD simulations have also shown a drawback of docking studies in considering protein as a rigid molecule. *In vivo* anticancer evaluation of **7e** showed that it has a potential to inhibit tumour growth and incidence through additional

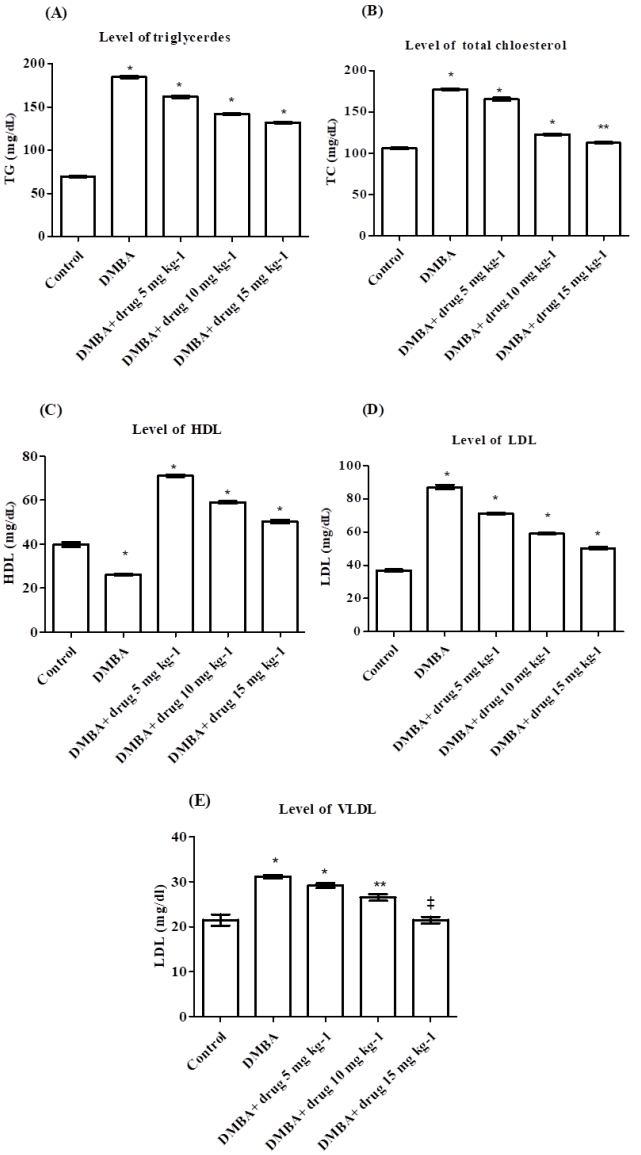

Figure 14. Effect of the **7e** derivative on the lipid level profile of treated and control group A statistically significant difference in means in comparison to control is marked by a symbol: * $p < 0.01$, # $p < 0.05$, ‡ $p > 0.05$.

mechanisms of action, such as modulating the antioxidant status and biotransformation enzymes. In this regard, the **7e** derivative is an excellent lead compound with efficiency similar to that of erlotinib. Since this compound is based on a different scaffold, it represents an opportunity to develop structurally different EGFR inhibitors, which could be used in the case of cancer resistance to drugs already in use. Additional studies are in progress to further optimise these drug-like characteristics and will be reported in due course.

Experimental Section

Chemistry

General

All experiments were carried out using commercial reagents and analytical grade solvents without further purification. Melting points of the derivatives

was determined using Veego (MPI melting point instrument). ^{1}H NMR and ^{13}C NMR analysis were performed using JEOL 300 and Bruker Avance II 100 NMR spectrometers respectively, with CDCl3 as solvent and TMS as the internal standard. Mass spectra was obtained using the VG-AUTOSPEC spectrometer equipped with ESI source (Fisons Instruments, Manchester, UK). Elemental analysis was carried out on Vario EL-III CHNOS elemental analyser (Elementar Analysensysteme, Hanau, Germany).

*Synthesis of 6,7-dibromo-2-methyl-4H-benzo[d][1,3]oxazin-4-one **(2)***
A mixture of 2-amino-4,5-dibromobenzoic acid (**1**) (0.05 mol) and acetic anhydride (0.1 mol) was refluxed under anhydrous conditions for 4 hours. The excess amount of acetic anhydride was distilled under reduced pressure and reaction mixture was cooled to room temperature. The intermediate benzoxazine-4-one was obtained as a solid mass and was used immediately in the next step (melting point: 173-175 ºC, yield: 84%).

*Synthesis of 3-(4-aminophenyl)-6,7-dibromo-2-methylquinazolin-4(3H)-one **(3)***
6,7-dibromo-2-methyl-4H-benzo[d][1,3]oxazin-4-one (**2**) (0.01 mol) was refluxed with *p*-phenylenediamine (0.01 mol) in presence of pyridine (15 ml) for 3 hours with occasional shaking. The reaction mixture was then cooled to room temperature. The crystals were filtered, rinsed with water, and dried. The product formed was recrystallized from ethyl acetate. The obtained product was a dark brown solid. Yield: 79% (3.2 g, 7.82 mmol); molecular formula: $C_{15}H_{11}Br_2N_3O$; melting point: 220-222 ºC; molecular weight: 409.08; ^{1}H NMR (300 MHz, $CDCl_3$, TMS) δ ppm: 2.26 (s, 3H, CH_3), 4.52 (s, 2H, NH_2), 6.85 (d, 2H, J = 6.9 Hz, 2xCH, Ar); 7.14 (d, 2H, J = 7.2 Hz, 2xCH, Ar); 7.49 (s, 1H, quinazoline), 8.062 (s, 1H, quinazoline); ^{13}C NMR (100 MHz, $CDCl_3$) δ ppm: 24.5, 117.7, 122.0, 124.5, 127.4, 124.5, 128.8, 130.6, 134.5, 148.1, 154.1, 156.1, 160.6.

*Synthesis of 4,6-dichloro-2-piperazin-1-yl-[1,3,5]triazine **(5)** and disubstituted 1,3,5-triazine **(6a-n)***
The derivatives **5** and **6(a-n)** were synthesized as described in our previous research.[31,32,62]

*Synthesis of 6,7-dibromo-2-methyl-3-(4-((4-(substitutedamino)-6-(piperidin-1-yl)-1,3,5-triazine-2yl)amino)phenyl)quinazolin-4(3H)-one (**7a-n**)*
0.01 mol of 3-(4-aminophenyl)-6,7-dibromo-2-methylquinazolin-4(3H)-one (**3**) and 0.01 mol of previously synthesized disubstituted 1,3,5-triazine derivatives (**6a–n**) were dissolved in 25 ml of 1,4-dioxane. Further, 0.01 mol of K_2CO_3 and a pinch of tin granules (as catalyst) were added into the reaction mixture and refluxed for 6-8 hours with continuous stirring. The excess solvent was evaporated under reduced pressure and recrystallized from ethanol to obtain the pure product.

*1-(4-((4-(6,7-dibromo-2-methyl-4-oxoquinazolin-3(4H)-yl)phenyl)amino)-6-(piperidin-1-yl)-1,3,5-triazin-2-yl)urea **(7a)***
Dark brown solid; yield 72% (4.5 g, 7.15 mmol); molecular formula: $C_{24}H_{23}Br_2N_9O_2$; melting point: 230-232 ºC; molecular weight: 629.32; ^{1}H NMR (300 MHz, $CDCl_3$, TMS) δ ppm: 1.57 (m, 4H, 2xCH_2, piperidine), 1.68 (m, 2H, CH_2, piperidine), 2.26 (s, 3H, CH_3), 3.75 (t, 4H, 2xCH_2, piperidine), 6.20 (s, 2H, NH_2), 7.25 (d, 2H, J = 7.5 Hz, 2xCH, Ar), 7.30 (d, 2H, J = 7.2 Hz, 2xCH, Ar), 7.49 (s, 1H, quinazoline), 8.062 (s, 1H, quinazoline), 8.34 (s, 1H, NH), 8.95 (s, 1H, NH); ^{13}C NMR (100 MHz, $CDCl_3$) δ ppm: 23.7, 24.5, 25.5, 54.8,117.7, 122.0, 127.4, 124.5, 128.8, 130.6, 134.5, 148.1, 154.1; MS (m/z): 629.7 $[M+H]^+$; elemental analysis: calculated C: 45.81%, H: 3.68%, N: 20.03%; found C: 45.94%, H: 3.32%, N: 20.10%.

*1-(4-((4-(6,7-dibromo-2-methyl-4-oxoquinazolin-3(4H)-yl)phenyl)amino)-6-(piperidin-1-yl)-1,3,5-triazin-2-yl)thiourea **(7b)***
Light brown solid; yield 75% (4.8 g, 7.44 mmol); molecular formula: $C_{24}H_{23}Br_2N_9OS$; melting point: 210-212 ºC; molecular weight: 645.38; ^{1}H NMR (300 MHz, $CDCl_3$, TMS) δ ppm: 1.57 (m, 4H, 2xCH_2, piperidine), 1.68 (m, 2H, CH_2, piperidine), 2.26 (s, 3H, CH_3), 3.75 (t, 4H, 2xCH_2, piperidine), 7.25 (d, 2H, J = 7.5 Hz, 2xCH, Ar), 7.30 (d, 2H, J = 7.2 Hz, 2xCH, Ar), 7.49 (s, 1H, quinazoline), 8.06 (s, 1H, quinazoline), 8.34 (s, 1H, NH), 9.13 (s, 2H, NH_2), 9.65 (s, 1H, NH); ^{13}C NMR (100 MHz, $CDCl_3$) δ ppm: 23.7, 24.5, 25.5, 54.8, 117.7, 122.4, 124.5, 127.4, 128.8, 130.6, 134.5, 148.1, 154.1, 160.6, 165.7, 171.7, 176.0, 181.4; MS-ESI (m/z): 645.6 $[M+H]^+$; elemental analysis: calculated C: 44.67%, H: 3.59%, N: 19.53%; found C: 45.05%; H: 3.25%; N: 19.90%.

*6,7-dibromo-2-methyl-3-(4-((4-(phenylamino)-6-(piperidin-1-yl)-1,3,5-triazin-2-yl)amino)phenyl) quinazoline-4(3H)-one **(7c)***
Black solid; yield 75% (4.9 g, 7.40 mmol); molecular formula: $C_{29}H_{26}Br_2N_8O$; melting point: 228-230 ºC; molecular weight: 662.39; ^{1}H NMR (300 MHz, $CDCl_3$, TMS) δ ppm: 1.57 (m, 4H, 2xCH_2, piperidine), 1.68 (m, 2H, CH_2, piperidine), 2.26 (s, 3H, CH_3), 3.75 (t, 4H, 2xCH_2, piperidine), 7.01 (t, 1H, CH, Ar), 7.2 (d, 2H, J = 7.2 Hz, 2xCH, Ar), 7.30 (d, 2H, J = 7.2 Hz, 2xCH, Ar), 7.35 (t, 2H, 2xCH, Ar), 7.49 (s, 1H, CH, quinazoline), 7.74 (d, 2H, J = 8.4 Hz, 2xCH, Ar), 8.34 (s, 1H, NH), 8.91 (s, 1H, NH); ^{13}C NMR (100 MHz, $CDCl_3$) δ ppm: 23.7, 24.5, 25.5, 54.8, 117.7, 122.4, 122.4, 124.5, 127.4, 128.8, 129.5, 130.6, 134.5, 134.5, 138.9, 148.1, 154.1, 160.6, 165.7, 168.9, 176; MS-ESI (m/z): 662.6 $[M+H]^+$; elemental analysis: calculated C: 52.59%, H: 3.96%, N: 16.92%; found C: 52.94%, H: 3.65%, N: 16.72%.

*6,7-dibromo-3-(4-((4-((4-chlorophenyl)amino)-6-(piperidin-1-yl)-1,3,5-triazin-2-yl)amino)phenyl)-2-methylquinazolin-4(3H)-one **(7d)***
Black solid: yield 85% (5.9 g, 8.47 mmol); molecular formula: $C_{29}H_{25}Br_2ClN_8O$; melting point: 270-272 ºC; molecular weight: 696.83; ^{1}H NMR (300 MHz, $CDCl_3$, TMS) δ ppm: 1.57 (m, 4H, 2xCH_2, piperidine), 1.68 (m, 2H, CH_2, piperidine), 2.26 (s, 3H, CH_3), 3.75 (t, 4H, 2xCH_2, piperidine), 7.20 (d, 2H, J = 6.6 Hz, 2xCH, Cl-Ar), 7.25 (d, 2H, J = 6.8 Hz, 2xCH, Ar), 7.30 (d, 2H, J = 6.9 Hz, 2xCH, Ar), 7.49 (s, 1H, CH, quinazoline), 7.53 (d, 2H, J = 6.6 Hz, 2xCH, Cl-Ar), 8.06 (s, 1H, CH, quinazoline), 8.34 (s, 1H, NH), 8.91 (s, 1H, NH); ^{13}C NMR (100 MHz, $CDCl_3$) δ ppm: 23.7, 24.5, 25.5, 54.8, 117.7, 122, 122.1, 122.4, 124.5, 127.4, 128.8, 129.6, 130.6, 134.5, 137, 148.1, 154.1, 160.6, 165.7, 168.9, 176; MS-ESI (m/z): 696.2 $[M+H]^+$; elemental analysis: calculated C: 49.99%, H: 3.62%, N: 16.08%; found C: 49.45%, H: 3.25%, N: 15.86%.

*6,7-dibromo-2-methyl-3-(4-((4-morpholino-6-(piperidin-1-yl)-1,3,5-triazin-2-yl)amino)phenyl) quinazoline-4(3H)-one **(7e)***
White solid; yield 76% (4.9 g, 7.47 mmol); molecular formula: $C_{27h28}Br_2N_8O_2$; melting point: 260-262 ºC; molecular weight: 656.38; ^{1}H NMR (300 MHz, $CDCl_3$, TMS) δ ppm: : 1.57 (m, 4H, 2xCH_2, piperidine), 1.68 (m, 2H, CH_2, piperidine), 2.26 (s, 3H, CH_3), 3.68 (t, 4H, 2xCH_2, morpholine), 3.79 (t, 4H, 2xCH_2, piperidine), 3.75 (t, 4H, 2xCH_2, morpholine), 7.25 (d, 2H, J = 6.3 Hz, 2xCH, Ar), 7.30 (d, 2H, J = 6.6 Hz, 2xCH, Ar), 7.69 (s, 1H, CH, quinazoline), 8.06 (s, 1H, CH, quinazoline), 8.34 (s, 1H, NH); ^{13}C NMR (100 MHz, $CDCl_3$) δ ppm: 23.7, 24.5, 25.5, 25.5, 48.7, 54.8, 66.3, 117.7, 122, 122.4, 124.5, 127.4, 128.8, 130.6, 134.5, 148.1, 154.1, 160.6, 168.9, 176, 179.2; MS-ESI (m/z): 656.2 $[M+H]^+$; elemental analysis: calculated C: 49.41%, H: 4.30%; N: 17.07%; found C: 49.10%; H: 4.60%; N: 17.15%.

*6,7-dibromo-3-(4-((4,6-di(piperidin-1-yl)-1,3,5-triazin-2-yl)amino)phenyl)-2-methylquinazolin-4(3H)-one **(7f)***

Dark brown solid; yield 69% (4.5 g, 6.88 mmol); molecular formula: $C_{28}H_{30}Br_2N_8O$; melting point: 220-222 ºC; molecular weight: 654.41; ^{1}H NMR (300 MHz, $CDCl_3$, TMS) δ ppm: 1.57 (m, 8H, 4xCH_2, piperidine), 1.68 (m, 4H, 2xCH_2, piperidine), 2.26 (s, 3H, CH_3), 3.75 (t, 8H, 4xCH_2, piperidine), 7.25 (d, 2H, J = 6.3 Hz, 2xCH, Ar), 7.30 (d, 2H, J = 6.9 Hz, 2xCH, Ar), 7.49 (s, 1H, CH, quinazoline), 8.06 (s, 1H, CH, quinazoline), 8.34 (s, 1H, NH); ^{13}C NMR(100 MHz, $CDCl_3$) δ ppm: 23.7, 24.5, 25.5, 54.8, 54.8, 117.7, 122, 122.4, 127.4, 128.8, 130.6, 134.5, 148.1, 154.1, 160.6, 168.9, 177.6; MS-ESI (m/z): 654.4 $[M+H]^+$; elemental analysis: calculated C: 51.39%, H: 4.62%, N: 17.12%; found C: 51.20%, H: 4.60%; N: 17.05%.

6,7-dibromo-3-(4-((4-((4-methoxyphenyl)amino)-6-(piperidin-1-yl)-1,3,5-triazin-2-yl)amino)phenyl)-2-methylquinazolin-4(3H)-one ***(7g)***

Brown solid; yield 82% (5.6 g, 8.09 mmol); molecular formula: $C_{30}H_{28}Br_2N_8O_2$; melting point: 265-267 ºC; molecular weight: 692.42; ^{1}H NMR (300 MHz, $CDCl_3$, TMS): 1.57 (m, 4H, 2xCH_2, piperidine), 1.68 (m, 2H, CH_2, piperidine), 2.26 (s, 3H, CH_3), 3.81 (s, 3H, OCH_3), 3.75 (t, 4H, 2xCH_2, piperidine), 6.93 (d, 2H, J = 7.8 Hz, methoxy-Ph), 7.25 (d, 2H, J = 6.3 Hz, 2xCH, Ar), 7.30 (d, 2H, J = 6.6 Hz, 2xCH, Ar), 7.49 (s, 1H, CH, quinazoline), 7.66 (d, 2H, J = 6.9 Hz, methoxy-Ph), 8.06 (s, 1H, CH, quinazoline), 8.34 (s, 1H, NH), 8.91 (s, 1H, NH); ^{13}C NMR (100 MHz, $CDCl_3$) δ ppm: 24.5, 54.8, 55.8, 115.1, 117.7, 122, 122.4, 124.5, 127.4, 128.8, 130.6, 131.2, 134.5, 148.1, 153.3, 154.1, 160.6, 165.7, 168.9, 176; ; MS-ESI (m/z): 692.8 $[M+H]^+$; elemental analysis: calculated C: 52.04%, H: 4.08%, N: 16.18%; found C: 52.10%, H: 4.10%, N: 16.40%.

2-(4-((4-(6,7-dibromo-2-methyl-4-oxoquinazolin-3(4H)-yl)phenyl)amino)-6-(piperidin-1-yl)-1,3,5-triazin-2-yl)hydrazine-1-carbothioamide ***(7h)***

Light brown solid; yield 74% (4.8 g, 7.27 mmol); molecular formula: $C_{24}H_{24}Br_2N_{10}OS$; melting point: 258-260 ºC; molecular weight: 660.39; ^{1}H NMR (300 MHz, $CDCl_3$, TMS) δ ppm 1.57 (m, 4H, 2xCH_2, piperidine), 1.68 (m, 2H, CH_2, piperidine), 2.26 (s, 3H, CH_3), 3.75 (t, 4H, 2xCH_2, piperidine), 7.25 (d, 2H, J = 6.3 Hz, 2xCH, Ar), 7.30 (d, 2H, J = 7.8 Hz, 2xCH, Ar), 7.49 (s, 1H, CH, quinazoline), 8.06 (s, 1H, CH, quinazoline), 8.34 (s, 1H, NH), 9.13 (s, 2H, NH_2), 9.65 (s, 1H, NH); ^{13}C NMR (100 MHz, $CDCl_3$) δ ppm: 21.7, 24.5, 25.5, 54.8, 117.7, 122, 124.5, 127.4, 128.8, 130.6, 134.5, 134.5, 148.1, 154.1, 160.6, 165.7, 174.3, 182.5; MS-ESI (m/z): 660.9 $[M+H]^+$; elemental analysis: calculated C: 52.65%, H: 4.66%, N: 21.21%; found C: 52.40%, H: 4.42%, N: 21.45%.

2-(4-((4-(6,7-dibromo-2-methyl-4-oxoquinazolin-3(4H)-yl)phenyl)amino)-6-(piperidin-1-yl)-1,3,5-triazin-2-yl)hydrazine-1-carboxamide ***(7i)***

Light brown solid; yield 71% (4.5 g, 6.98 mmol); molecular formula: $C_{24}H_{24}Br_2N_{10}O_2$; melting point: 262-264 ºC; molecular weight: 644.33; ^{1}H NMR (300 MHz, $CDCl_3$, TMS) δ ppm: 1.57 (m, 4H, 2xCH_2, piperidine), 1.68 (m, 2H, CH_2, piperidine), 2.26 (s, 3H, CH_3), 3.75 (t, 4H, 2xCH_2, piperidine), 6.22 (s, 2H, NH_2), 7.25 (d, 2H, J = 6.3 Hz, 2xCH, Ar), 7.30 (d, 2H, J = 6.9 Hz, 2xCH, Ar), 7.49 (s, 1H, CH, quinazoline), 8.06 (s, 1H, CH, quinazoline), 8.34 (s, 1H, NH), 9.13 (s, 1H, NH); ^{13}C NMR (100 MHz, $CDCl_3$) δ ppm: 23.7, 24.5, 25.5, 54.8, 117.7, 122, 122.4, 124.5, 127.4, 128.8, 130.6, 134.5, 148.1, 154.1, 157.4, 160.6, 165.7, 182.9; MS-ESI (m/z): 644.8 $[M+H]^+$; elemental analysis: calculated C: 44.74%, H: 3.75%, N: 24.74%; found C: 44.45%, H: 3.50%, N: 24.85%.

6,7-dibromo-3-(4-((4-((4-bromophenyl)amino)-6-(piperidin-1-yl)-1,3,5-triazin-2-yl)amino)phenyl)-2-methylquinazolin-4(3H)-one ***(7j)***

Brown solid; yield 79% (5.8 g, 7.82 mmol); molecular formula: $C_{29}H_{25}Br_3N_8O$; melting point: 276-278 ºC; molecular weight: 741.29; ^{1}H NMR (300 MHz, $CDCl_3$, TMS) δ ppm: 1.57 (m, 4H, 2xCH_2, piperidine), 1.68 (m, 2H, CH_2, piperidine), 2.26 (s, 3H, CH_3), 3.75 (t, 4H, 2xCH_2, piperidine), 7.01 (d, 2H, J = 6.3 Hz, 2xCH, Br-Ar), 7.25 (d, 2H, J = 6.3 Hz, 2xCH, Ar), 7.30 (d, 2H, J = 6.9 Hz, 2xCH, Ar), 7.408 (d, 2H, J = 7.2 Hz, 2xCH, Br-Ar), 7.49 (s, 1H, CH, quinazoline), 8.06 (s, 1H, CH, quinazoline), 8.34 (s, 1H, NH), 8.91 (s, 1H, NH); ^{13}C NMR (100 MHz, $CDCl_3$) δ ppm: 23.7, 24.5, 25.5, 54.8, 116.7, 117.7, 118.5, 122, 122.4, 124.5, 127.4; MS-ESI (m/z): 640.9 $[M+H]^+$; elemental analysis: calculated C: 46.99%, H: 3.40%, N:15.12%; found C: 46.64%, H: 3.50%, N: 15.50%.

6,7-dibromo-2-methyl-3-(4-((4-((4-nitrophenyl)amino)-6-(piperidin-1-yl)-1,3,5-triazin-2-yl)amino)phenyl)quinazolin-4(3H)-one ***(7k)***

Yellowish-white solid; yield 74% (5.2 g, 7.35 mmol); molecular formula: $C_{29}H_{25}Br_2N_9O_3$; melting point: 265-267 ºC; molecular weight: 707.39; ^{1}H NMR (300 MHz, $CDCl_3$, TMS) δ ppm: 1.57 (m, 4H, 2xCH_2, piperidine), 1.68 (m, 2H, CH_2, piperidine), 2.26 (s, 3H, CH_3), 3.75 (t, 4H, 2xCH_2, piperidine), 7.25 (d, 2H, J = 6.3 Hz, 2xCH, Ar), 7.30 (d, 2H, J = 6.6 Hz, 2xCH, Ar), 7.46 (d, 2H, J = 6.3 Hz, 2xCH, nitro-Ar), 7.49 (s, 1H, CH, quinazoline), 8.032 (d, 2H, J = 6.3 Hz, 2xCH, nitro-Ar), 8.06 (s, 1H, CH, quinazoline), 8.34 (s, 1H, NH), 9.13 (s, 1H, NH); ^{13}C NMR (100 MHz, $CDCl_3$) δ ppm: 23.7, 24.5, 25.5, 54.8, 117.7, 117.7, 119.2, 122.4, 124.5, 124.7, 127.4, 128.8, 130.6, 134.5, 137.9, 145, 148.1, 154.1, 160.6, 165.7, 168.9, 176; MS-ESI (m/z): 707.9 $[M+H]^+$; elemental analysis: calculated C: 49.24%, H: 3.56%, N: 17.82; found C: 49.28%, H: 3.82%, N: 17.70%.

6,7-dibromo-2-methyl-3-(4-((4-(methylamino)-6-(piperidin-1-yl)-1,3,5-triazin-2-yl)amino)phenyl) quinazolin-4(3H)-one ***(7l)***

Light brown solid; yield 69% (4.1 g, 6.83 mmol); molecular formula: $C_{24}H_{24}Br_2N_8O$; melting point: 206-208 ºC; molecular weight: 600.32; ^{1}H NMR (300 MHz, $CDCl_3$, TMS) δ ppm: 1.57 (m, 4H, 2xCH_2, piperidine), 1.68 (m, 2H, CH_2, piperidine), 2.26 (s, 3H, CH_3), 2.92 (s, 3H, CH_3), 3.75 (t, 4H, 2xCH_2, piperidine), 7.25 (d, 2H, J = 6.3 Hz, 2xCH, Ar), 7.30 (d, 2H, J = 7.2 Hz, 2xCH, Ar), 7.49 (s, 1H, CH, quinazoline), 7.96 (s, 1H, NH), 8.06 (s, 1H, CH, quinazoline), 8.34 (s, 1H, NH); ^{13}C NMR (100 MHz, $CDCl_3$) δ ppm: 23.7, 24.5, 25.5, 28.5, 54.8, 117.7, 122, 122.4, 124.5, 127.4, 128.8, 130.6, 134.5, 148.1, 154.1, 160.6, 165.7, 165.7, 176; MS-ESI (m/z): 600.1 $[M+H]^+$; elemental analysis: calculated C: 48.02%, H: 4.03%, N: 18.67%; found C: 48.08%, H: 3.90%, N: 18.60%.

*3-(4-((4-amino-6-(piperidin-1-yl)-1,3,5-triazin-2-yl)amino)phenyl)-6,7-dibromo-2-methylquinazolin-4(3H)-one (****7m****)*

Yellowish solid; yield 64% (3.75 g, 6.40 mmol); molecular formula: $C_{23}H_{22}Br_2N_8O$; melting point: 267-269 ºC; molecular weight: 586.29; ^{1}H NMR (300 MHz, $CDCl_3$, TMS) δ ppm: 1.57 (m, 4H, 2xCH_2, piperidine), 1.68 (m, 2H, CH_2, piperidine), 2.26 (s, 3H, CH_3), 3.75 (t, 4H, 2xCH_2, piperidine), 6.94 (s, 2H, NH_2), 7.25 (d, 2H, J = 6.3 Hz, 2xCH, Ar), 7.30 (d, 2H, J = 6.9 Hz, 2xCH, Ar), 7.49 (s, 1H, CH, quinazoline), 8.06 (s, 1H, CH, quinazoline), 8.34 (s, 1H, NH); ^{13}C NMR (100 MHz, $CDCl_3$) δ ppm: 23.7, 24.5, 25.5, 54.8, 117.7, 122, 122.4, 124.5, 127.4, 128.8, 130.6, 134.5, 148.1, 154.1, 160.6, 165.7, 176, 182.4; MS-ESI (m/z): 586.4 $[M+H]^+$; elemental analysis: calculated C: 47.12%, H: 3.78%, N: 19.11%; found C: 47.02%, H: 3.50%, N: 19.25%.

*4-((4-((4-(6,7-dibromo-2-methyl-4-oxoquinazolin-3(4H)-yl)phenyl)amino)-6-(piperidin-1-yl)-1,3,5-triazin-2-yl)amino)benzoic acid (****7n****)*

Brown solid; yield 68% (4.8 g, 6.80 mmol); molecular formula: $C_{30}H_{26}Br_2N_8O_3$; melting point: 272-274 ºC; molecular weight: 706.40; ^{1}H NMR (300 MHz, $CDCl_3$, TMS) δ ppm: 1.57 (m, 4H, 2xCH_2, piperidine), 1.68 (m, 2H, CH_2, piperidine), 2.26 (s, 3H, CH3), 3.75 (t, 4H, 2xCH_2, piperidine), 7.25 (d, 2H, J = 6.3 Hz, 2xCH, Ar), 7.30 (d, 2H, J = 6.3 Hz, 2xCH, Ar), 7.49 (s, 1H, CH, quinazoline), 7.73 (d, 2xCH, J = 6.6 Hz, Ar), 8.03 (d, 2H, J = 6.3 Hz, 2xCH, Ar), 8.06 (s, 1H, CH, quinazoline), 8.34 (s, 1H, NH), 8.914 (s, 1H, NH), 12.712 (s, 1H, OH, Ar); ^{13}C NMR (100 MHz, $CDCl_3$) δ ppm: 23.7, 24.5, 25.5, 54.8, 111.2, 117.7, 120.2, 122, 122.4, 124.5, 127.4, 128.8,

130.6, 131.1, 134.5, 144.1, 148.1, 154.1, 160.6, 165.7, 168.9, 169.3, 176; MS-ESI (m/z): 706.2 $[M+H]^+$; elemental analysis: calculated C: 51.01%, H: 3.71%, N: 15.86%; found C: 51.02%, H: 3.40%, N: 15.60%.

Pharmacological assays

In vitro anticancer assays

The synthesized derivatives were screened for their anti-cancer activity against four different cell lines: MCF-7 (human breast cancer cell line), HeLa (human cervical cancer cell line), HL-60 (human promyelocytic leukaemia cell line), and HepG2 (human hepatic cancer cell line). As a cytotoxicity control, two normal human cell lines, HFF (human foreskin fibroblast cell line) and MCF-12A (normal epithelial breast cell line) were used.

Cell cultures

The selected cancer and normal cell lines were maintained (1×10^4 cells/well) in monolayer cultures in a supplemented Dulbecco's modified eagle's medium (DMEM) with 10% heat-inactivated foetal bovine serum (FBS), 1% L-glutamine, and 50 µg/mL gentamycin sulphate, at 37 ºC, in a CO_2 incubator in an atmosphere of humidified 5% CO_2 and 95% air.

Preparation of samples

Derivatives were dissolved in DMSO and 1 mg/mL concentration solutions were prepared. The derivatives were then diluted with DMEM and 10% FBS, after which the solutions were filtered and sterilized, using a 0.2 µM syringe filter to prepare working solutions. Further dilutions (1–100 µM) were made, again followed by filtration and sterilization.

Cytotoxic activity measurement

In vitro cytotoxic activities of synthesized derivatives were determined using the MTT assay. Different concentrations of derivatives (diluted in the culture medium), were added into the wells with respective controls and incubated for 48 hours. After that, 10 mL of MTT (3-(4,5-dimethylthiazol-2-yl)-2,5-diphenyl tetrazolium bromide) (5 mg/mL) was added into each well and the plates were further incubated for 4 hours. Then the supernatant from each well was carefully removed, and formazan crystals were dissolved in 100 mL of DMSO, after which absorbance at 540 nm was recorded.[31,32,49] All calculations were carried out in duplicate. Determination of cell viability (%) is calculated using the following formula:

$$Cell\ viability\ (\%) = \frac{Mean\ OD\ (sample)}{Mean\ OD\ (control)} \times 100 \quad (1)$$

Where OD represents optical density. Determination of IC_{50} values was obtained by statistical analysis.

EGFR inhibitory activity

Kinase-Glo® Plus (luminescent kinase assay) kit was used to determine EGFR inhibitory activity of the synthesized derivatives. The assay is based upon quantification of the remaining ATP in the solution of the kinase reaction, which is inversely correlated to the luminescent signal.[63] In the assay, a stock solution of the derivatives (100 mM in 10% DMSO) were prepared and serially diluted (10 nM to 500 nM). Further, 5 mL of the diluted solution was added to a 50 mL of the reaction mixture (10 mM $MgCl_2$, 40 mM Tris, pH 7.4, 0.1 mg/mL BSA, 0.2 mg/mL Poly (Glu, Tyr) substrate, 10 mM ATP and EGFR (50 nM)). Enzymatic reactions were allowed to proceed for 40 minutes at 30 °C, after which the plates were incubated for 5 minutes at room temperature and 50 mL of Kinase-Glo® Plus kit solution was added into each 96-well plate. The reaction mixture was again incubated at 30 °C for 30 minutes. After the incubation period, 25 mL of ADP-Glo reagent was added to terminate the assay, which was followed by shaking of the plates for 30 minutes at ambient temperature, incubating them, and adding 50 mL of the kinase detection reagent. Reading of the plates was performed using the ADP-Glo Luminescence reader. The same procedure was also performed for the control. The corrected activity results were calculated as the difference between the tested and control samples for each protein kinase target and IC_{50} were calculated by the standard equation.[32,49,63]

In ovo antiangiogenic activity on cancer induced chorioallantoic membrane (CAM)

Fertilized chicken eggs (480 in total) were obtained from a local commercial hatchery and the dirt was removed mechanically using a 70% denatured ethanol. Eggs were then placed into a rotating incubator (37 °C, 60% relative humidity for 10 days, 4 rotation/hour) for embryogenesis. Each of the incubation days was termed as an embryo development day (EDD). On the third EDD, the eggs were placed on their side in an egg rack. A torch was used to candle for the blunt end of the air sac. The chorioallantoic vein and its large blood vessels junctions were marked. A 1 cm^2 box was drawn approximately 1 cm away from the branch point of the vein. The marked area was then cleaned with iodine and drills into the marked area were made using a rotating cutting tool. A small hole was made in the eggshell membrane using a 25 gauge syringe, being careful not to tear the underlying CAM. The CAM was subsequently detached from the eggshell membrane using gentle suction created by an automatic pipette (fitted with a piece of ¼" tygon tubing) by placing it against the hole in the air sac. The process of suction was carried out in such a way that the air pocket was underneath the hole in the square, signifying that the CAM has been successfully detached from the eggshell. The air sac and the square near the chorioallantoic vein were then sealed with a semi-transparent laboratory tape. On EDD 8, the seal was removed, and a 4 mm radial disc was placed on the chorioallantoic membrane of each egg. The eggs were then resealed and incubated for the next 24 hours at the same conditions.

A selected tumour cell line (MCF-7) was detached from its culture dish using EDTA:PBS (1:10 v/v) to remove the excess residual media. MCF-7 cells (4×10^4 cells) were placed on the top of uncoated 12 µm ring inserts. Eggs were put in the upright position for at least 6 hours, allowing the migration of the cancer cells into the lower chamber.

Synthesized derivatives (1.0 µM) were prepared in PBS. 10 µL of these solutions was added directly to the disk on top of CAM. At higher doses of tested and reference compounds the immunity of the chicken embryos was found to be compromised and the integrity of the CAM was at risk. Therefore, lower concentration (1 µM) of the test and standard compounds were used.[31,32,64]

Activity measurements were done by counting the number of blood vessels in the area under the disk using a stereo microscope. Eggs that showed inflammation and embryo-toxicity due to experimental error were excluded. The experiment was done in triplicate and each test sample was tested on 10 different eggs to measure cumulative inhibition score.[65,66] Antiangiogenic scores were calculated using the formula:

$$Average\ Score = \frac{(N_1+N_2)\times2}{N} \quad (2)$$

Where N is a total number of eggs where a derivative showed weak, strong or no effect, N_1 is a total number of eggs where a derivative showed a medium effect, N_2 is a total number of eggs where a derivative showed a strong effect. The score patterns of semi-quantitative results are as follows:

0: no or weak effect (more than 150 new blood vessels).

1: medium effect (between 50 and 150 new blood vessels).

2: strong effect (between 0 and 50 new blood vessels or the capillary-free zone is at least twice as large as the pallet).

Docking studies

Docking studies were performed using AutoDock Vina,[67] which uses dispersion, hydrogen bonds, electrostatic, and desolvatation components for determination of the most probable complex conformation. 3D coordinates of the EGFR kinase domain complexed with lapatinib (PDB entry 1XKK)[56] and erlotinib (PDB entry 4HJO)[68] were taken from RCSB Protein Data Bank. Water molecules were omitted from the structures, hydrogen atoms were added were necessary, and all Lys, Arg, His and Cys side chains were protonated, while all Asp and Glu side chains were deprotonated and both amino and carboxyl ends were charged using the UCSF Chimera 1.14. program (University of California, USA),[69] which was also used for results visualization and interpretation. Additionally, all missing amino acid residues were added according to Šali and Bundell's Modeller service[50] accessed through UCSF Chimera 1.14. Initial 3D conformation of all ligands (**7a**-**7n**) was determined using HyperChem 8.0 (Hypercube, Inc., Gainesville, FL, USA). A grid map of size 22.5 × 22.5 × 22.5 Å was generated by the AutoGrid program[70] and centred on the coordinates of one of the nitrogen atoms of lapatinib's quinazoline ring (12.683, 33.305, 37.276). The receptor molecule was regarded as rigid while all ligands' single bonds could rotate freely. Docking procedure was run with exhaustiveness set to 100. The validity of the approach was assessed by lapatinib redocking using 4 different conditions (neutral lapatinib moiety and the charged moiety most prevalent at pH 7.4, without water molecules and in presence of HOH 4 and HOH 22 water molecules, which are located inside the binding site). The charge of the ligand was calculated according to Ionescu *et al*.[71]

Molecular dynamics (MD) simulations

Docked positions of erlotinib and four ligands with the highest affinities for binding to EGFR were used as starting points for MD simulations. AMBER ff14SB force field was used to model the enzyme and GAFF force field was used in the case of ligands. Such protein-ligand complexes were solvated in a truncated octahedral box of TIP3P water molecules spanning a 12 Å thick buffer, neutralized by Na^+ ions and submitted to geometry optimization in AMBER16 program,[72] employing periodic boundary conditions in all directions. For the first 1500 cycles the complex was restrained and only water molecules were optimized, after which another 2500 cycles of optimization followed where both water molecules and the complex were unrestrained. Optimized systems were gradually heated from 0 to 300 K and equilibrated during 30 ps using NVT conditions, followed by productive and unconstrained MD simulations of 300 ns employing a time step of 2 fs at a constant pressure (1 atm) and temperature (300 K), the latter held constant using Langevin thermostat with a collision frequency of 1 ps^{-1}. Bonds involving hydrogen atoms were constrained using the SHAKE algorithm,[73] while the long-range electrostatic interactions were calculated employing the Particle Mesh Ewald method.[74] The nonbonded interactions were truncated at 11.0 Å. Analysis of the trajectories was performed using the cpptraj module of AmberTools16.[75]

Binding free energy calculations and decomposition

The binding energy, ΔG_{bind}, of simulated complexes was calculated using the MM-GBSA (Molecular Mechanics – Generalized Born Surface Area) protocol,[58,76] available as a part of AmberTools16.[72] MM-GBSA is a method for the calculation of ΔG_{bind} from snapshots of MD trajectory[77] with an estimated standard error of 1–3 kcal/mol.[58] ΔG_{bind} is calculated in the following manner:

$$\Delta G_{bind} = < G_{complex} > - < G_{protein} > - < G_{ligand} > \quad (3)$$

Where the symbol < > represents the average value over 1000 snapshots collected from the last 30 ns of the corresponding MD trajectories. The calculated MM-GBSA binding free energies were decomposed into specific residue contribution on a per-residue basis according to established procedures. This protocol calculates the contributions to ΔG_{bind} arising from each amino acid side chains and identifies the nature of the energy change in terms of interaction and solvation energies.[78,79] Due to the similarity of the compounds, the entropic component of ΔG_{bind} was not calculated.

In vivo anticancer pharmacology

Animal model

Female Sprague-Dawley (SD) rats, weighing between 100 and 150 g, were used for the study after approval from the Institutional Animal Ethics Committee. The animals were kept in suitable cages at 25 °C, with 45–55% humidity and 12/12 hours light/dark cycles under standard atmosphere with free access to food and water. The entire protocol for conducting the animal studies was reviewed and approved by the Institutional Animal Ethics Committees (IAEC) for the Purpose of Control and Supervision of Experiments on Animals, Government of India (1546/PO/E/S/11/CPCSEA).

Oral toxicity study

The dose of the **7e** derivative was estimated using an acute toxicity study in healthy SD rats (6–8 weeks old) as per OECD Guideline-423. The rats were fasted overnight with water ad libitum. A dose of 5, 10, 20 30, and 40 mg of the **7e** derivative per kilogram of body weight was introduced orally to the rats. After administration of the drug, the rats were observed at least once during the first 2 hours and then again after 24 and 48 hours for any behavioural changes or death. Since animals did not exhibit any toxic symptoms, behaviour changes or mortality up to 30 mg/kg of body weight during the observation period, doses of 5 mg/kg, 10 mg/kg, and 15 mg/kg were selected for the study.

Induction of breast cancer

7,12-dimethylbenz(a) anthracene (DMBA) is a polycyclic aromatic hydrocarbon which induces cancer through formation of epoxides, which bind to DNA and form DNA adducts and lead to erroneous DNA transcription.[49,80] Breast cancer was induced with a single 25 mg subcutaneous DMBA injection (emulsified in sunflower oil and saline) near the mammary gland.

Experimental design

A total number of 30 animals was randomly divided into five groups, with each group containing six animals. Different groups received different treatments as follows:

Group I: Animals were treated with a 0.9% w/v of NaCl solution and served as the untreated control.

Groups II: Animals were treated with a single subcutaneous injection of DMBA (25 mg) near the mammary gland. This group served as a negative control without any drug treatment.

Group III: DMBA + derivative (**7e**) at a dose of 5 mg/kg once per day throughout the experimental period.

Group IV: DMBA + derivative (**7e**) at a dose of 10 mg/kg once per day throughout the experimental period.

Group V: DMBA + derivative (**7e**) at a dose of 15 mg/kg once per day throughout the experimental period.

A free access to water and food was supplied during the entire experiment and the body weight of all animals was regularly monitored. On the final day (end of the 16th week), all animals were kept fasted overnight and sacrificed by cervical dislocation under ether anaesthesia. Blood samples

of all animals were collected by puncturing the retro-orbital sinus plexus and were kept in labelled centrifuge tubes. Plasma was separated by centrifuge (10,000 rpm for 15 minutes). Selected tissues (liver and mammary glands) were immediately excised and homogenized using 0.1 M Tris-HCl buffer (pH 7.4) at 4 °C and centrifuged. The resulting clear homogenates were collected for biochemical assays.[81,82]

Biochemical assays

Determination of plasma and mammary TBARS, LOOH, and antioxidant parameters such as SOD, CAT, GPX, GSH, CYP, Cyt-b5, GST, GR, and the levels of TC, TG, HDL, LDL, and VLDL in the plasma were done on the basis of previous reported methods with minor modifications.[83–97]

Statistical analysis

Data are expressed as mean ± SEM for each group. Statistical analysis was done using GraphPad Prism version 5.0 software. One-way analysis of variance (ANOVA) followed by Dunnett's t-test was used to compare effectiveness of synthesized derivatives and the reference drug or control.

Acknowledgements

A part of the work was supported by Act 211 Government of the Russian Federation, contract 02.A03.21.0011 and by the Ministry of Science and Higher Education of Russia (Grant FENU-2020-0019). Authors are also sincerely thankful to Department of Pharmaceutical sciences, SHUATS, Allahabad, Uttar Pradesh, India and Laboratory of Computational Modelling of Drugs, Higher Medical and Biological School, South Ural State University, Chelyabinsk, Russia for experimental and computational research facilities. Authors also acknowledge University of Zagreb, University Computing Centre (SRCE) for granting computational time on the ISABELLA cluster.

Conflict of interest

The authors declare no conflict of interest.

Keywords: EGFR inhibitors • synthesis • molecular modelling • *in vitro* assays • *in vivo* assays

[1] E. Zwick, J. Bange, A. Ullrich, *Endocr. Relat. Cancer* **2001**, 161–173.

[2] A. C. Porter, R. R. Vaillancourt, *Oncogene* **1998**, *17*, 1343–1352.

[3] J. D. Jordan, E. M. Landau, R. Iyengar, *Cell* **2000**, *103*, 193–200.

[4] P. Blume-Jensen, T. Hunter, *Nature* **2001**, *411*, 355–365.

[5] A. Wells, *Int. J. Biochem. Cell Biol.* **1999**, *31*, 637–643.

[6] L. V. Sequist, T. J. Lynch, *Annu. Rev. Med.* **2008**, *59*, 429–442.

[7] J. E. Dancey, *Cancer Cell* **2004**, *5*, 411–415.

[8] S. V. Sharma, D. W. Bell, J. Settleman, D. A. Haber, *Nat. Rev. Cancer* **2007**, *7*, 169–181.

[9] D. S. Krause, R. A. Van Etten, *N. Engl. J. Med.* **2005**, *353*, 172–187.

[10] M. Nadeem Abbas, S. Kausar, F. Wang, Y. Zhao, H. Cui, *Cells* **2019**, *8*, 350–372.

[11] R. I. Nicholson, J. M. W. Gee, M. E. Harper, *Eur. J. Cancer* **2001**, *37*, S9–S15.

[12] E. D. Adamson, in *Curr. Top. Dev. Biol.*, Elsevier, **1990**, pp. 1–29.

[13] A. M. Partanen, in *Curr. Top. Dev. Biol.*, Elsevier, **1990**, pp. 31–55.

[14] P. R. Dutta, A. Maity, *Cancer Lett.* **2007**, *254*, 165–177.

[15] C. R. M. Asquith, K. M. Naegeli, M. P. East, T. Laitinen, T. M. Havener, C. I. Wells, G. L. Johnson, D. H. Drewry, W. J. Zuercher, D. C. Morris, *J. Med. Chem.* **2019**, *62*, 4772–4778.

[16] R. Akhavan Sigari, M. R. Gaab, V. Rohde, M. Abili, H. Ostertag, *Anticancer Res.* **2014**, *34*, 623–30.

[17] K. N. Ganjoo, H. Wakelee, *Biol. Targets Ther.* **2007**, *1*, 335–346.

[18] K. Abouzid, S. Shouman, *Bioorg. Med. Chem.* **2008**, *16*, 7543–7551.

[19] M. T. Conconi, G. Marzaro, L. Urbani, I. Zanusso, R. Di Liddo, I. Castagliuolo, P. Brun, F. Tonus, A. Ferrarese, A. Guiotto, A. Chilin, *Eur. J. Med. Chem.* **2013**, *67*, 373–383.

[20] A. E. Wakeling, S. P. Guy, J. R. Woodburn, S. E. Ashton, B. J. Curry, A. J. Barker, K. H. Gibson, *Cancer Res.* **2002**, *62*, 5749–5754.

[21] G. M. Higa, J. Abraham, *Expert Rev. Anticancer Ther.* **2007**, *7*, 1183–1192.

[22] S. L. Greig, *Drugs* **2016**, *76*, 263–273.

[23] M. Cheng, X. Yu, K. Lu, L. Xie, L. Wang, F. Meng, X. Han, X. Chen, J. Liu, Y. Xiong, J. Jin, *J. Med. Chem.* **2020**, *63*, 1216–1232.

[24] Q. Li, T. Zhang, S. Li, L. Tong, J. Li, Z. Su, F. Feng, D. Sun, Y. Tong, X. Wang, Z. Zhao, L. Zhu, J. Ding, H. Li, H. Xie, Y. Xu, *ACS Med. Chem. Lett.* **2019**, *10*, 869–873.

[25] H. Park, H. Y. Jung, S. Mah, S. Hong, *Angew. Chemie* **2017**, *129*, 7742–7746.

[26] J. Shen, T. Zhang, S. J. Zhu, M. Sun, L. Tong, M. Lai, R. Zhang, W. Xu, R. Wu, J. Ding, C. H. Yun, H. Xie, X. Lu, K. Ding, *J. Med. Chem.* **2019**, *62*, 7302–7308.

[27] M. J. Morin, *Oncogene* **2000**, *19*, 6574–6583.

[28] Y. Xia, Z. Y. Yang, M. J. Hour, S. C. Kuo, P. Xia, K. F. Bastow, Y. Nakanishi, P. Nampoothiri, T. Hackl, E. Hamel, K. H. Lee, *Bioorg. Med. Chem. Lett.* **2001**, *11*, 1193–1196.

[29] S. T. Al-Rashood, I. A. Aboldahab, M. N. Nagi, L. A. Abouzeid, A. A. M. Abdel-Aziz, S. G. Abdel-hamide, K. M. Youssef, A. M. Al-Obaid, H. I. El-Subbagh, *Bioorg. Med. Chem.* **2006**, *14*, 8608–8621.

[30] N. M. Raghavendra, P. M. Gurubasavarajaswamy, K. S. Nagaranavile, T. Parameshwaran, *Arch. Pharm. Res.* **2009**, *32*, 431–436.

[31] P. Pathak, P. K. Shukla, V. Kumar, A. Kumar, A. Verma, *Inflammopharmacology* **2018**, *26*, 1441–1453.

[32] Prateek, Pathak, V. Naumovich, M. Grishina, P. Kumar, Shukla, Amita, Verma, Vladimir, Potemkin, *Arch. Pharm. (Weinheim).* **2019**, *352*, 1–18.

[33] F. Zuccotto, E. Ardini, E. Casale, M. Angiolini, *J. Med. Chem.* **2010**, *53*, 2681–2694.

[34] Y. Liu, N. S. Gray, *Nat. Chem. Biol.* **2006**, *2*, 358–364.

[35] C. S. Tan, N. B. Kumara Kulasinghe, Y. Q. Huang, Y. L. E. Ang, J. R. E. Choo, B. C. Goh, R. A. Soo, *Mol. Cancer* **2018**,

17, 1–14.

[36] D. N. Do Amaral, J. Lategahn, H. H. Fokoue, E. M. B. da Silva, C. M. R. Sant Anna, D. Rauh, E. J. Barreiro, S. Laufer, L. M. Lima, *Sci. Rep.* **2019**, *9*, 14.

[37] J. Graham, M. Muhsin, P. Kirkpatrick, *Nat. Rev. Drug Discov.* **2004**, *3*, 11–12.

[38] G. E. Winter, D. L. Buckley, J. Paulk, J. M. Roberts, A. Souza, S. Dhe Paganon, J. E. Bradner, *Phthalimide Conjugation as a Strategy for in Vivo Target Protein Degradation*, **2015**.

[39] D. P. Bondeson, A. Mares, I. E. D. Smith, E. Ko, S. Campos, A. H. Miah, K. E. Mulholland, N. Routly, D. L. Buckley, J. L. Gustafson, N. Zinn, P. Grandi, S. Shimamura, G. Bergamini, M. Faelth-Savitski, M. Bantscheff, C. Cox, D. A. Gordon, R. R. Willard, J. J. Flanagan, L. N. Casillas, B. J. Votta, W. den Besten, K. Famm, L. Kruidenier, P. S. Carter, J. D. Harling, I. Churcher, C. M. Crews, *Nat. Chem. Biol.* **2015**, *11*, 611–617.

[40] D. P. Bondeson, B. E. Smith, G. M. Burslem, A. D. Buhimschi, J. Hines, S. Jaime Figueroa, J. Wang, B. D. Hamman, A. Ishchenko, C. M. Crews, *Cell Chem. Biol.* **2018**, *25*, 78-87.e5.

[41] P. Ottis, C. M. Crews, *ACS Chem. Biol.* **2017**, *12*, 892–898.

[42] P. M. Cromm, C. M. Crews, *Cell Chem. Biol.* **2017**, *24*, 1181–1190.

[43] M. Pettersson, C. M. Crews, *Drug Discov. Today Technol.* **2019**, *31*, 15–27.

[44] G. M. Burslem, B. E. Smith, A. C. Lai, S. Jaime Figueroa, D. C. McQuaid, D. P. Bondeson, M. Toure, H. Dong, Y. Qian, J. Wang, A. P. Crew, J. Hines, C. M. Crews, *Cell Chem. Biol.* **2018**, *25*, 67-77.e3.

[45] M. Couto, M. F. García, C. Alamón, M. Cabrera, P. Cabral, A. Merlino, F. Teixidor, H. Cerecetto, C. Viñas, *Chem. - A Eur. J.* **2018**, *24*, 3122–3126.

[46] G. W. Rao, G. J. Xu, J. Wang, X. L. Jiang, H. B. Li, *ChemMedChem* **2013**, *8*, 928–933.

[47] E. J. Hanan, M. Baumgardner, M. C. Bryan, Y. Chen, C. Eigenbrot, P. Fan, X. H. Gu, H. La, S. Malek, H. E. Purkey, G. Schaefer, S. Schmidt, S. Sideris, I. Yen, C. Yu, T. P. Heffron, *Bioorg. Med. Chem. Lett.* **2016**, *26*, 534–539.

[48] C. R. M. Asquith, K. A. Maffuid, T. Laitinen, C. D. Torrice, G. J. Tizzard, D. J. Crona, W. J. Zuercher, *ChemMedChem* **2019**, *14*, 1693–1700.

[49] J. K. Srivastava, G. G. Pillai, H. R. Bhat, A. Verma, U. P. Singh, *Sci. Rep.* **2017**, *7*, 1–18.

[50] A. M. Sieuwerts, J. G. M. Klijn, H. A. Peters, J. A. Foekens, *Clin. Chem. Lab. Med.* **1995**, *33*, 813–823.

[51] S. R. Mortensen, S. Brimijoin, M. J. Hooper, S. Padilla, *Toxicol. Appl. Pharmacol.* **1998**, *148*, 46–49.

[52] E. Damiani, J. A. Solorio, A. P. Doyle, H. M. Wallace, *Toxicol. Lett.* **2019**, *302*, 28–34.

[53] D. W. Fry, A. J. Bridges, W. A. Denny, A. Doherty, K. D. Greis, J. L. Hicks, K. E. Hook, P. R. Keller, W. R. Leopold, J. A. Loo, D. J. Mcnamara, J. M. Nelson, V. Sherwood, J. B. Smaill, S. Trumpp Kallmeyer, E. M. Dobrusin, *Proc. Natl. Acad. Sci. U. S. A.* **1998**, *95*, 12022–12027.

[54] A. Wang, X. Li, H. Wu, F. Zou, X. E. Yan, C. Chen, C. Hu, K. Yu, W. Wang, P. Zhao, J. Wu, Z. Qi, W. Wang, B. Wang, L. Wang, T. Ren, S. Zhang, C. H. Yun, J. Liu, Q. Liu, *J. Med. Chem.* **2017**, *60*, 2944–2962.

[55] J. Engel, A. Richters, M. Getlik, S. Tomassi, M. Keul, M. Termathe, J. Lategahn, C. Becker, S. Mayer Wrangowski, C. Grütter, N. Uhlenbrock, J. Krüll, N. Schaumann, S. Eppmann, P. Kibies, F. Hoffgaard, J. Heil, S. Menninger, S. Ortiz Cuaran, J. M. Heuckmann, V. Tinnefeld, R. P. Zahedi, M. L. Sos, C. Schultz Fademrecht, R. K. Thomas, S. M. Kast, D. Rauh, *J. Med. Chem.* **2015**, *58*, 6844–6863.

[56] E. R. Wood, A. T. Truesdale, O. B. McDonald, D. Yuan, A. Hassell, S. H. Dickerson, B. Ellis, C. Pennisi, E. Horne, K. Lackey, K. J. Alligood, D. W. Rusnak, T. M. Gilmer, L. Shewchuk, *Cancer Res.* **2004**, *64*, 6652–6659.

[57] M. M. Hamed, D. A. Abou El Ella, A. B. Keeton, G. A. Piazza, A. H. Abadi, R. W. Hartmann, M. Engel, *ChemMedChem* **2013**, *8*, 1495–1504.

[58] S. Genheden, U. Ryde, *Expert Opin. Drug Discov.* **2015**, *10*, 449–461.

[59] N. Homeyer, H. Gohlke, *Mol. Inform.* **2012**, *31*, 114–122.

[60] K. Karki, D. Pande, R. Negi, R. Khanna, H. D. Khanna, *Med. Sci.* **2016**, *4*, 17.

[61] T. Sun, J. Gao, D. Han, H. Shi, X. Liu, *Drug Deliv.* **2019**, *26*, 975–988.

[62] P. Pathak, A. Thakur, H. R. Bhat, U. P. Singh, *J. Heterocycl. Chem.* **2015**, *52*, 1108–1113.

[63] D. Balzano, S. Santaguida, A. Musacchio, F. Villa, *Chem. Biol.* **2011**, *18*, 966–975.

[64] C. S. Kue, K. Y. Tan, M. L. Lam, H. B. Lee, *Exp. Anim.* **2015**, *64*, 129–138.

[65] H. T. Kıyan, B. Demirci, K. H. C. Başer, F. Demirci, *Pharm. Biol.* **2014**, *52*, 44–50.

[66] L. Krenn, D. H. Paper, *Phytomedicine* **2009**, *16*, 1083–1088.

[67] O. Trott, A. J. Olson, *J. Comput. Chem.* **2009**, 455–461.

[68] J. H. Park, Y. Liu, M. A. Lemmon, R. Radhakrishnan, *Biochem. J.* **2012**, *448*, 417–423.

[69] E. F. Pettersen, T. D. Goddard, C. C. Huang, G. S. Couch, D. M. Greenblatt, E. C. Meng, T. E. Ferrin, *J. Comput. Chem.* **2004**, *25*, 1605–1612.

[70] G. M. Morris, R. Huey, W. Lindstrom, M. F. Sanner, R. K. Belew, D. S. Goodsell, A. J. Olson, *J. Comput. Chem.* **2009**, *30*, 2785–2791.

[71] C. M. Ionescu, D. Sehnal, F. L. Falginella, P. Pant, L. Pravda, T. Bouchal, R. Svobodová Vařeková, S. Geidl, J. Koča, *J. Cheminform.* **2015**, *7*, 50.

[72] D. A. Case, R. M. Betz, D. S. Cerutti, T. E. Cheatham III, T. A. Darden, R. E. Duke, T. J. Giese, H. Gohlke, A. W. Goetz, N. Homeyer, S. Izadi, P. Janowski, J. Kaus, A. Kovalenko, T. S. Lee, S. LeGrand, P. Li, C. Lin, T. Luchko, R. Luo, B. Madej, D. Mermelstein, K. M. Merz, G. Monard, H. Nguyen, H. T. Nguyen, I. Omelyan, A. Onufriev, D. R. Roe, A. Roitberg, C. Sagui, C. L. Simmerling, W. M. Botello Smith, J. Swails, R. C. Walker, J. Wang, R. M. Wolf, X. Wu, L. Xiao, P. A. Kollman, *Univ. California, San Fr.* **2016**.

[73] J. P. Ryckaert, G. Ciccotti, H. J. C. Berendsen, *J. Comput. Phys.* **1977**, *23*, 327–341.

[74] T. Darden, D. York, L. Pedersen, *J. Chem. Phys.* **1993**, *98*, 10089–10092.

[75] D. R. Roe, T. E. Cheatham, *J. Chem. Theory Comput.* **2013**,

9, 3084–3095.

[76] T. Hou, J. Wang, Y. Li, W. Wang, *J. Chem. Inf. Model.* **2011**, *51*, 69–82.

[77] G. G. Ferenczy, in *Thermodyn. Kinet. Drug Bind.* (Eds.: G.M. Keserü, D.C. Swinney), Wiley-VCH Verlag GmbH & Co. KGaA, Weinheim, Germany, **2015**, pp. 37–61.

[78] G. Rastelli, A. Del Rio, G. Degliesposti, M. Sgobba, *J. Comput. Chem.* **2009**, *32*, 797–810.

[79] H. Gohlke, C. Kiel, D. A. Case, *J. Mol. Biol.* **2003**, *330*, 891–913.

[80] D. Chakravarti, D. Venugopal, P. C. Mailander, J. L. Meza, S. Higginbotham, E. L. Cavalieri, E. G. Rogan, *Mutat. Res. Toxicol. Environ. Mutagen.* **2008**, *649*, 161–178.

[81] A. Y. Nasr, *Toxicol. Reports* **2014**, *1*, 682–691.

[82] J. A. de Meneses, C. A. J. Lopes, C. Velarde, T. G. Boaventura, *Nutr Hosp.* **2011**, *26*, 716–721.

[83] H. Ohkawa, N. Ohishi, K. Yagi, *Anal. Biochem.* **1979**, *95*, 351–358.

[84] J. Folch, M. Lees, G. Sloane Stanley, *J Biol Chem.* **1957**, *226*, 497-509.

[85] A. Zlatkis, B. Zak, A. Boyle, *J Lab Clin Med.* **1953**, *41*, 486-492.

[86] R. Foster, LB Dunn, *Clin Chem.* **1973**, *19*, 338-340.

[87] K. Falholt, B. Lund, W. Falholt, *Clin. Chim. Acta* **1973**, *46*, 105–111.

[88] A. Zilversmit, DB Davis, *Laboratorio* **1950**, *10*, 127-135.

[89] Z. Y. Jiang, J. V. Hunt, S. P. Wolff, *Anal. Biochem.* **1992**, *202*, 384–389.

[90] P. Kakkar, B. Das, P. N. Viswanathan, *Indian J Biochem Biophys.* **1984**, *21*, 130-132.

[91] A. K. Sinha, *Anal. Biochem.* **1972**, *47*, 389–394.

[92] J. T. Rotruck, A. L. Pope, H. E. Ganther, A. B. Swanson, D. G. Hafeman, W. G. Hoekstra, *Selenium: Biochemical Role as a Component of Glutathione Peroxidase*, **1973**.

[93] E. Beutler, B. M. Kelly, *Experientia* **1963**, *19*, 96–97.

[94] T. Omura, R. Sato, *Biol Chem.* **1964**, *239*, 2370-2378.

[95] W. Habig, M. Pabst, W. Jakoby, *J Biol Chem.* **1974**, *249*, 7130-7139.

[96] I. Carlberg, B. Mannervik, **1985**, pp. 484–490.

10.1002/cmdc.202000646

WILEY-VCH

FULL PAPER

Entry for the Table of Contents